Title: Advanced Measurement Techniques for Braided Composite Structures: A Review of Current and Upcoming Trends

Garrett W. Melenka[1*], Cagri Ayranci[2]

[1]Lassonde School of Engineering, York University, 4700 Keele St. North York, ON M3J 1P3

[2]Mechanical Engineering, University of Alberta, Donadeo Innovation Centre for Engineering, 9211-116 Street NW, Edmonton AB Canada T6G 1H9

*corresponding author: gmelenka@yorku.ca

Abstract

Braiding is an advanced textile manufacturing method that is used to produce two dimensional (2D) and three dimensional (3D) components. Unlike a laminated structures braids have interlaced yarns that forms a continuity between layers. This structure allows for improved impact resistance, damage tolerance and improved through-thickness reinforcement. Despite the numerous advantages of braided composites, braids also have shortcomings. Their highly complex fiber architecture presents challenges in the availability and choice of the strain measuring and characterization techniques. Advanced measurement methods such as optical strain measurement, micro-computed tomography, and in-situ strain measurement are required. Optical strain measurement methods such as digital image correlation and high speed imaging are necessary to accurately measure the complex deformation and failure that braided composites exhibit. X-ray based micro-computed tomography measurements can provide detailed geometric and morphologic information for braided structures which is necessary for accurately predicting the mechanical properties of braided structures. Finally, in-situ strain measurement methods will provide detailed information on the internal deformation and strain that exists within braided structures. In-situ sensors will also allow for in-service health monitoring of braided structures. This paper provides a detailed review of the aforementioned sensing technologies and their relation to the measurement of braided composite structures.

Keywords:

Braided composites, digital image correlation, micro-computed tomography, structural health monitoring

1 Introduction

Braided composites are part of the textile composites family of composite materials [1], [2]. Braiding is used to form geometries by interweaving yarns into a preform architecture [3]. Braided composites are then formed by impregnating the braided preform with a matrix material. Braided composites contain two major classes: two dimensional (2D) and three dimensional (3D) braids [4]. 2D braided composites are produced using a device known as a Maypole braider that can be used to produce mainly cylindrical (or tubular) products, but it is also possible to produce flat or axisymmetric structures altering the machine components or the mandrels used during production. 2D braided composites are composed of yarns placed in a biaxial configuration with respect to the longitudinal direction of the braids (i.e. at $\pm\theta^{\circ}$ angles). Additional axial fiber yarns can be placed in the longitudinal direction in a braided structure to form tri-axially braided composite structures when increased axial or bending stiffness and strength is required [5]. 3D braided composites, on the other hand, are produced using Cartesian or rotary braiding machines which produce components with through thickness fiber reinforcement [2], [6]. Cartesian machines are designed in a column-track (or column-row) arrangement where carriers of the yarns are moved in a continuous manner by advancing columns and rows systematically in a back and forth manner. Rotary 3D braiding machines are similar to that of the Maypole machines in design with the exception that the carriers are not only arranged and move in a circular pattern, but they also move in the thickness direction [7]. Schematics of a Maypole braiding machine and a Cartesian braiding machine are shown in Figure 1. Examples of 2D braided composite structures (representative schematic unit cells) are shown in Figure 2 are biaxial, triaxial and 3D braided composites.

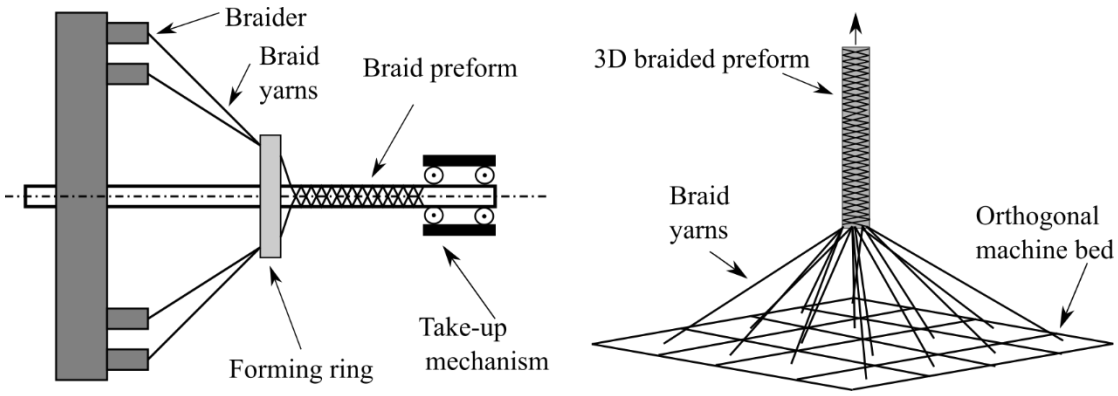

Figure 1: Example braiding machines Left: Maypole braider Right: Cartesian braider

Both braiding techniques are versatile manufacturing methods that can be used to create complex fiber architectures with 2D or 3D structures. A major challenge with braided composites is the complex undulating nature of yarns (indicated in Figure 2 for both 2D and 3D braids) within the braided structures. There exists a significant amount of literature on the predictive modeling of braided composite structures [8]–[10]. Analytical and numerical models have been utilized to predict the elastic properties of braided structures. Models have also been created to analyze damage and failure of braided structures [11], [12]. Finite element analysis (FEA) models have also been extensively developed for braided composites [13]–[16].

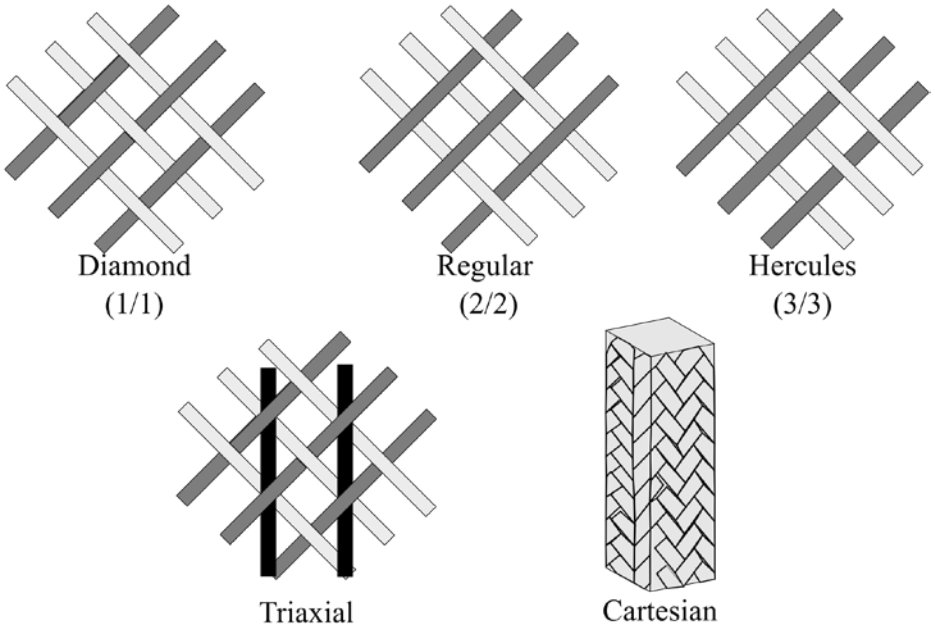

Figure 2: Examples of schematic drawings of 2D and 3D (Cartesian) braided composite structures

To complement the advanced modeling methods that exist for braided composites accurate measurement techniques are also required. These techniques are necessary to thoroughly characterize the deformations and strains that occurs in the braided structures. Accurate measurements of both internal and external strains provide vital data for numerical and analytical model development and validation. This is particularly important to allow for the increased use of braided structures in structural, aerospace, automotive, and biomedical applications.

Measurements of braid deformation and strains is not only necessary within the elastic loading zone of the materials, but also in the plastic and/or failure zones. Failure and damage that occurs to braided composite structures is also difficult to predict and assess due to the interwoven nature of braided composites. 2D braided composites exhibit a “scissoring” behavior where deformation of the braid yarns within the braided structure can occur under loading [17]. Additionally, braids exhibit progressive failure which includes failure modes such as matrix failure, delamination and fiber failure [18]–[21]. Presently, a number of numerical models have been developed to

investigate the failure and damage of braided structures [22]. Accurate measurement methods are also crucial to fully characterize the complex damage and failure behavior of braided structures.

This paper is intended to provide a review of the current and upcoming advanced measurement methods used for braided composites. Review will serve as a guide to researchers involved in experimental analysis of braided composites. Advanced topics for the analysis of braided composites covered here include: contact free strain measurement, in-situ strain measurement, micro-structural analysis, structural health monitoring, and braid geometry analysis. These advanced measurements are necessary to gain further insights into the complex behavior of braided structures. Improved measurement methods will lead to the improvement and development of models for predicting the behavior of advanced braided composite structures. Specific advanced measurement methods covered in this review for braided composite structures are digital image correlation, computed tomography, acoustic emission, optical fiber sensors and co-braided sensing yarns/fibers.

2 Optical Strain Measurement for Braided Composites

Fundamental understanding of braided composites was initially developed using conventional strain gauges. Fundamental analysis for understanding the effect of unit cell size and number of unit cells needed to obtain accurate strain measurements were done using strain gages [23], [24]. Building on this knowledge, in recent years, digital image correlation (DIC) has become an established technique for accurate strain measurement [25]. DIC is particularly advantageous for the strain measurement of braided composites due to their non-homogeneous structural nature [26]. The DIC measurement can be applied in two configurations. Two dimensional (2D) DIC utilizes a single camera as the strain measurement device and 2D deformation and strain (in-plane) is measured using this approach. Three dimensional (3D) DIC utilizes a pair of cameras in a stereo-

camera configuration to measure 3D deformation and strain (in-plane and out-of-plane). The 3D DIC measurement method is useful for the strain measurement of objects with complex geometries or for structures that exhibit in-plane as well as out-of-plane deformation and strain. The 3D DIC measurement method also provides redundant strain measurement since two sensors are utilized with this approach.

One major advantage of the DIC measurement over conventional strain measurement methods is the ability to use optics to change the field-of-view of the measurement camera. By changing camera optics varying regions of deformation and strain can be measured using the same camera. Additionally, this is a full-field measurement method that allows for strain over the camera field-of-view to be measured. The DIC measurement method can also be applied to a variety of different loading condition which further demonstrates the versatility of this measurement approach [26].

2.1 2D Digital Image Correlation

A schematic of the 2D DIC measurement setup is shown in Figure 3. The schematic shows the camera used for strain measurement, test sample with applied speckle pattern and white light illumination. The 2D DIC measurement method can be applied to a multitude of test configurations for planar test specimen. Example measurements that can be performed include: uniaxial tension, uniaxial compression, in-plane shear, and bending. The ability to perform a multitude of measurements demonstrates the versatility of the DIC measurement process.

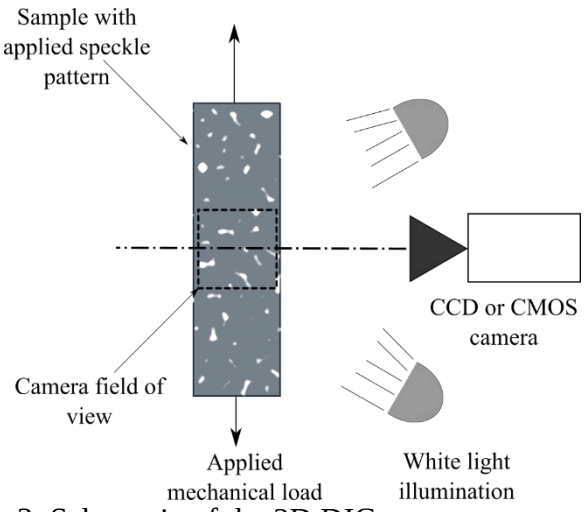

Figure 3: Schematic of the 2D DIC measurement method

As can be seen in Figure 3 the 2D DIC measurement is best used for the measurement of flat or planar test samples. Out of plane deformation and strain should be considered before using the 2D DIC measurement method. Longitudinal, transverse and shear strain can be measured for a planar test sample.

Several authors have used the 2D DIC measurement method for braided composite structures. El-Hajjar *et al.* used the 2D DIC measurement method to measure strain for glass fiber triaxial braided composite structures [27]. A commercial measurement system, Dantec DIC measurement system, was used by the authors for strain measurement. In this work, the axial and transverse strain results obtained from full field strain measurements were used to validate a closed form model to predict the elastic properties of tri-axially braided composite structures. Similarly, Qamhia *et al.* utilized the 2D DIC measurement method for the measurement of braided cellulose reinforced composites [28]. Samples were tested under tensile loads by both El-Hajjar *et al.* and Qamhia *et al.* [27], [28].

Kier *et al.* utilized the 2D DIC measurement method to evaluate triaxially braided composites under two loading conditions: tensile and shear loading [29]. The study by Kier *et al.* illustrates the versatility of the DIC measurement method as it can easily be configured for tensile or shear

strain measurement. Braid samples tested under shear load were fabricated to create v-notched samples to perform shear strain of braided composites. The v-notched test samples used in the study by Keir *et al*. are shown in Figure 4. The gauge section of the v-notched shear sample and example speckle pattern is shown in this figure. Braid samples were evaluated over a range of 30, 45 and 60° braiding angles. The outcome of the strain measurement was used to compare with a developed analytical and finite element analysis model.

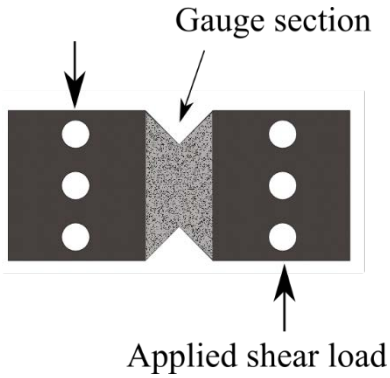

Figure 4: Example v-notched sample examined by Kier *et al.* for the shear properties of braided composites [29].

The work of Johnston *et al.* examined carbon fiber braids with a 0/60/-60° braid structure [30]. Four sample arrangements were used: Transverse bow-tie, compression, tension, v-notch shear. The results from this study demonstrated the effect loading conditions on the resulting strain fields exhibited for braided structures. Samples also were tested under three temperature conditions (i) room condition, (ii) hot (100°C), and (iii) hot/wet condition (60°C/90% RH). The result of the study by Johnston *et al.* found a 19% decrease in failure stress due to environmental conditions. Contact free measurement methods demonstrated that edge effects increase with environmental conditions.

2.2 3D Digital Image Correlation

To allow for both in-plane and out-of-plane strain measurement a 3D strain measurement method is required. A schematic of the 3D DIC measurement method is shown in Figure 5. In this

arrangement two cameras are used to collect images of the test sample. The two cameras are separated by an angle, α, which can typically range from 20-30° [31], [32]. The 3D DIC measurement technique has been used extensively for the measurement of composite structures [33].

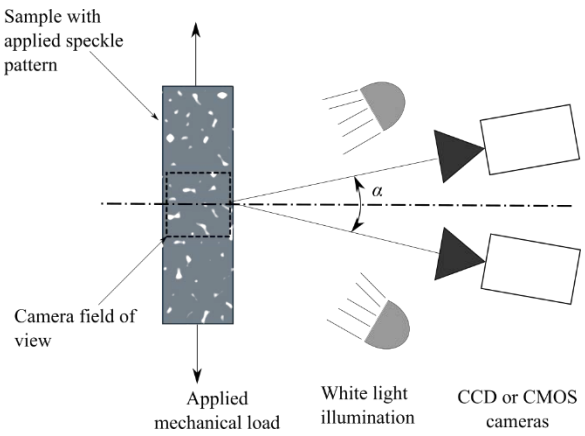

Figure 5: Schematic of the 3D DIC measurement method

Fouinneteau & Pickett were one of the first researchers to utilize a 3D DIC measurement technique for braided composite structures [34]. Flat braid samples manufactured using carbon and e-glass fibers were tested under tensile loads. The results obtained from the DIC measurements were used towards the development of a meso-mechanical damage model for braided composite structures. The highly complex post-failure strain data at the failure locations of the specimens were crucial in development and validation of the complex model developed by the authors. Conventional strain measuring techniques usually provide localized data that can not always be placed on the exact failure location. Most often conventional sensors do not survive aggressive failure of braided composites; consequently, use of 3D DIC system was extremely valuable for this study.

Leung *et al.* performed 3D DIC measurement of tubular braided composite samples using a stereo microscope [35]. The stereo microscope in conjunction with two cameras allowed for the three dimensional deformation and strain of a single braid unit cell to be measure. A unit cell is a small

repeating unit that is often used to describe the overall braided composite geometry. Authors indicated that the use of the 3D DIC measurement with a stereo microscope demonstrates the ability to measure localized strain for braided composite structures. The study by Leung *et al.* demonstrates that 3D strain can be measured on a microscale level for braided composite structures.

Cichosz and Wehrkamp-Richter evaluated triaxial braided composites using the 3D DIC measurement method [36], [37]. Samples manufactured with 30, 45 and 60° braid angles. Uniaxial tensile tests were performed at different off-axis orientations for each of the test samples. The use of the full-field 3D DIC measurement method allowed for the comparison of the strain field of the braid samples under a variety of loading conditions. Failure and damage of braided composite samples was examined using samples with off-axis loads.

The tensile response of carbon-aramid 3D braided composite was investigated by Zheng *et al.* [38]. Four hybrid braid performs were produced using a four-step 3D braiding process. An ARAMIS 3D DIC measurement system was used to evaluate the three dimensional deformation and strain of the 3D braided structures. The 3D DIC measurement results were used to demonstrate the effect of the hybrid braiding method on the tensile response of the produced braided structures.

A comprehensive examination of braided composite structures was performed by Melenka & Carey [39]. In this work, samples were evaluated with three different braiding angles: 35, 45 and 55°. In addition, the strain fields of two different braiding patterns were examined: Diamond (1/1) and Regular (2/2). Samples were evaluated using both tensile and torsional loading. The results from this work demonstrate the repeating strain fields that occur for braided composite structures. The effect of braiding pattern and braiding angle were explored. Representative strain fields for a

35° Diamond and Regular braids are shown in Figure 6. This figure demonstrated the effect of braid pattern and braiding angle on the on strain due to an applied axial load.

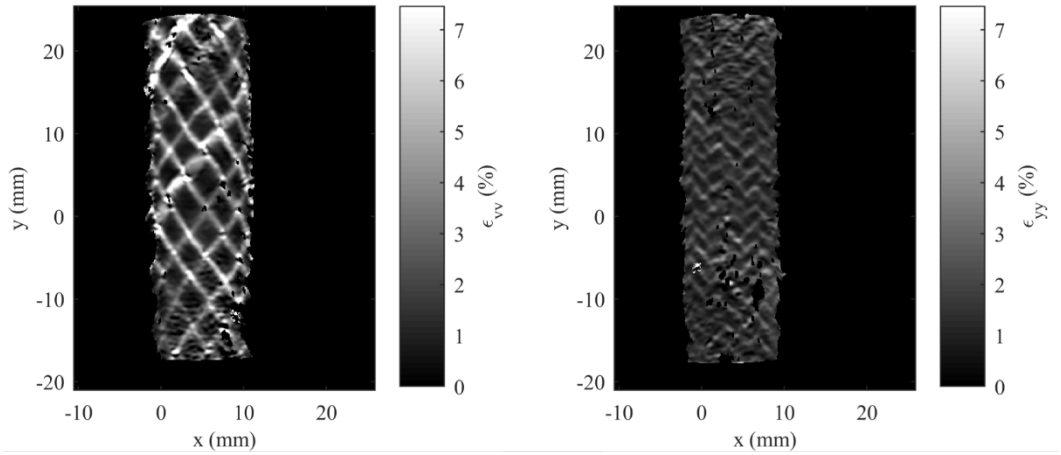

Figure 6: Representative strain field for Diamond (1/1) and Regular (2/2) braided composite structures

2.3 Braided Composites and High Speed Imaging

Braided composites exhibit high damage tolerance and impact resistance compared to conventional composite structures [19], [40]. Advanced measurement methods are necessary to evaluate the damage characteristics of 2D and 3D braided structures. High speed imaging is required to examine the high strain rate behavior of braided structures. High speed imaging can be used in a qualitative manner to visually assess the effect of damage on braided structures or can be coupled with the DIC image processing method.

The strain rate behaviour of 2D biaxial and triaxial braided composite was examined by Böhm *et al.* [41]. Five braid geometries were examined, three 2D biaxial braids and two 2D triaxial braids. Biaxial braids were manufactured with braiding angles of 30, 45 and 70° while triaxial braids were manufactured using 30 and 45° braiding angles. A high speed camera and the ARAMIS DIC measurement software was utilized to examine the high strain response of the braided structures.

Strain rates of 2, 10, 100 and 1000 mm/s were used for each braid sample. Testing was performed on flat braided composite structures. The stiffness and strength of 2D biaxial and triaxial braids were found to be strain rate dependent.

The energy absorption of reinforced braided composite structures was explored by Dorival *et al.* [42]. This study was one of the few braided composite work that studied the energy absorption using digital imaging. Dynamic crush tests were preformed using a drop weight tower with a mass of 4 kg and velocity of 6.5 m/s. A high speed camera and DIC analysis software was used to examine deformation and crushing behavior of the braided composite structure. A schematic of the test specimen geometry used for this study is shown in Figure 7. The test geometries consisted of an external 2D braided structure with a foam core. Different reinforcing geometries were evaluated. High speed imaging was used to examine the effect of different reinforcing designs on impact absorption and damage. A variety of reinforcing configurations were explored and the crush behaviors of each of the reinforced structures was examined.

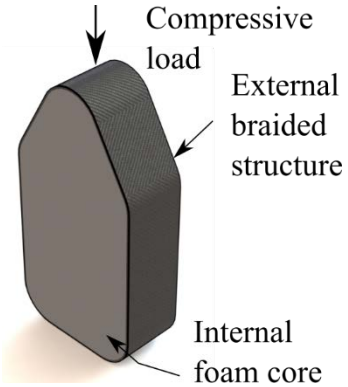

Figure 7: Sample for high speed crush testing. Adapted from Dorival *et al.* [42]

A novel application of the 3D DIC measurement method was performed by Pan *et al.* [43]. 3D braided composites were evaluated using high speed imaging. Strain measurement of the samples were performed using a high speed camera. A four mirror arrangement was utilized to achieve 3D strain measurement using a single high speed camera. A schematic of the four mirror high speed

imaging setup is shown in Figure 8. A 3D DIC measurement method was required to measure the 3D deformation and strain that occurs to the braided composite samples under impact loading. The methodology described allows for the 3D strain measurement of braided structures using a single high speed camera. The methodology presented by Pan *et al.* [43] overcomes two of major technical challenges for performing high speed 3D DIC measurement of braided composite structures. Firstly, using a single high speed camera removes the need of synchronizing multiple cameras. Secondly, the ability to use a single camera for 3D DIC measurement and high speed imaging drastically reduces the amount of data required for this measurement [41].

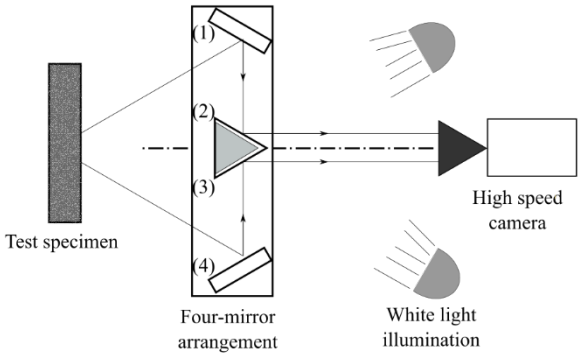

Figure 8: Example mirror arrangement to achieve stereo strain measurement using a single high-speed camera. Adapted from Pan *et al.* [43].

Damage and failure of triaxially braided composite structures was assess using high-speed imaging by Cichosz and Wehrkamp-Richter [36], [37]. The collected high-speed images were used to study the catastrophic failure that occurred to braid samples subjected to a multi-axis stress state. The evolution of damage and strain for braided structures was investigated. The braid samples examined in this study exhibited non-linear behavior prior to failure. The high speed camera allows for investigation of the catastrophic failure that braided composites exhibit under complex loading conditions. Good understanding of the mechanism may lead to developing braided

structures with pseudo-ductile failure characteristics by alteration of construction of the braids and/or use of hybrid fibers in the system [20], [21], [44], [45]

The high speed imaging systems used to evaluate braided composite structures are summarized in Table 1. The data presented in Table 1 can be used in the preparation of future high speed studies of braided composite structures. Furthermore, the methodologies described in Table 1 can be used in conjunction with DIC strain measurement methods.

Table 1: High speed imaging systems for braided composite samples

Author	Loading Rate	High Speed Camera	Camera Frame Rate	Sample Manufacturing Method
Böhm *et al.* [41]	2, 10, 100 and 1000 mm/s	Not Specified	Not Specified	Triaxial braided composites
Dorival *et al.* [42]	6.5 m/s	FastCAM-APX RS model 250k	20,000 Hz	2D braided composites
Pan *et al.* [43]	15 m/s	Photron Fas-tCam APXRS SA5	15,000-21,000 frames per second	3D braided composite
Cichosz and Wehrkamp-Richter [36], [37]	2 and 1.3 mm/s	Photron SA5	17,500 frames per second	Biaxial braided composite

2.4 DIC measurement methods for Braided Composites

2D DIC measurements provide full-field strain measurement for braided composite structures. Full field strain measurement allows for the visualization and analysis of strain field variations that occur due to the interwoven nature of braid yarns. Users can benefit from investigating a local versus global strain zone which is not always possible with other techniques that are available to the researchers. 2D DIC is an effective measurement tool for planar braid samples that do not exhibit out-of-plane displacement or strain. Samples that exhibit out-of-plane motion or have complex geometries require the ability to measure 3D deformation and strain.

A 2D DIC measurement experiment can affordably be constructed for braided composite measurement. Open-source DIC software such as Ncorr, DICe and YADICS [46]–[48] (Machine vision cameras and lenses suitable for DIC measurements can be purchased for approximately $2000 USD. Alternatively, commercial DIC software packages are also available such as: LaVision StrainMaster, Correlated Solutions VIC-2D or GOM ARAMIS. This demonstrates that a 2D DIC measurement can affordably be performed for braided structures.

Although a DIC measurement can easily be implemented for braided structures, this approach is not without drawbacks. A significant amount of image data is collected for DIC measurements. The DIC measurement can become impractical for evaluating large numbers of samples as a significant amount of data storage and processing time is required. The number of samples, number of images and test duration must be considered when designing a DIC measurement for braided structures. A single camera DIC system is only capable of measuring in-plane deformation and strain an additional camera is required to detect out-of-plane deformation.

The 3D DIC measurement technique is an effective tool for the measurement of the deformation and strain of advanced braided composite structures. In particular, the 3D DIC method is best

suited for samples which have complex 3D geometries or both in-plane and out-of-plane motion [31], [49]. Despite the many advantages of the 3D DIC measurement approach this technique is not without challenges. The 3D DIC method utilizes a pair of high resolution cameras as a result a significant amount of image data is collected for a single experiment. Data management and storage must be considered when designing a 3D DIC experiment. For composite structures with 3D geometries or that exhibit anisotropic behavior the 3D DIC measurement method is an effective tool for assessing the deformation and strain of 2D and 3D braided composite structures.

2.4.1 Sample Preparation for DIC Testing

When collecting images, reflections or bright spots that appear in the camera image must be minimized. Reflections or shiny surfaces will affect the accuracy of correlation results. To remove reflections preparation of the sample surface may be necessary. Surface reflection can be reduced, and image contrast can be improved by applying a flat black or flat white paint to the sample surface. Quick drying flat/matte black or flat white spray paints are recommended for preparing test sample surfaces. Matte paints will not produce a shiny or reflective surface. Paints should be chosen to be compatible with the matrix and fibers used to produce the braided structures.

Once the sample surface has been prepared a speckle pattern can be applied. The speckle pattern should provide a random contrast pattern to the test specimen surface. The speckle pattern size must be appropriate for the sample size and field of view. In general, speckles should be at least 5 pixels in diameter. The size of a speckle will depend on the image scale. For example, a 5 pixel speckle will correspond to a physical size of 0.25mm for an imaging setup with an image scale of 20 pixel/mm. Therefore, the speckle size and field of view must both be considered. Assessment of speckle pattern quality was examined by Lecompte *et al.* [50]. A detailed review of speckling pattern techniques is presented by Dong *et al.* where a variety of methods are described [51]. The choice of speckle pattern will depend on the size, geometry and material of the braided test specimen.

2.4.2 DIC Experimental setup and processing strategies for braided composites

The DIC measurement systems that were used to measure planar braided samples are summarized in Table 1. In this table the DIC software used for analysis, camera, and camera lens is listed. In

all of these studies the camera field of view and working distance is not listed. Furthermore, the DIC processing method (correlation window size) is also not listed for these studies. These parameters are necessary when examining braided composites as the choice of field of view depends highly on the unit cell geometry of the examined braided structure.

Table 2: Digital Image Correlation Measurement Systems for Planar Braided Composite Samples

Author	DIC System	Camera Resolution	Camera Lens	DIC Processing Method
El-Hajjar *et al.* [27]	Dantec Dynamics Q-400	5 megapixel camera	30mm Schneider Xenoplan Lens	Not specified
Qamhia *et al.* [28]	Dantec Dynamics Q-400	5 megapixel camera	30mm Schneider Xenoplan Lens	Not specified
Kier *et al.* [29]	ARAMIS	Grasshopper CCD Cameras	Not specified	Not specified
Johnston *et al.* [30]	ARAMIS	2 megapixel cameras	Not specified	Not specified

The 3D DIC measurement systems that were used to measure braided samples is summarized in Table 2. In this table the 3D DIC software used for analysis, camera, and camera lens is listed. The camera field of view and working distance is also detailed. The DIC processing strategies use for each study is also summarized. These parameters are necessary when examining braided

composites as the choice of field of view depends highly on the unit cell geometry of the examined braided structure.

Table 3: 3D Digital Image Correlation Measurement Systems for Braided Composite Samples

Author	DIC System	Camera Resolution	Camera Lens	Field of View	DIC Processing Method
Fouinneteau & Pickett [34]	Not Specified	2x 1.4 megapixel cameras	Not Specified	Not Specified	Not Specified
Leung *et al* [35]	LaVision Strain Master	2x 1376 x 1040 pixel Imager Intense Cameras	Zeiss Stereo Discovery V8 Microscope	~5.0 x 3.0 mm^2	256x256 first pass followed by 64x64 pixel subset with 75% offset
Cichosz and Wehrkamp-Richter [36], [37]	GOM ARAMIS	2x 4 Megapixel cameras	Not Specified	70 mm gauge length	17x17 pixel with 2 pixel overlap
Zheng *et al* [38]	GOM ARAMIS	2x 5 Megapixel Cameras Baumer TXG50	Titanar 50mm	25 x 85mm^2	Not Specified

Melenka & Carey [39]	LaVision Strain Master	2x AVT GT3400 9.1 Megapixel Cameras	LM35SC Kowa Lenses	39.3x 29.4mm^2	31 pixel subset with 8 pixel overlap

The DIC measurement methods provides significant information for the deformation and strain of braided composite structures. Since this is a full-field measurement method strain results can readily be compared with analytical and numerical FEA studies for model validation therefore complete experimental details are required for model validation.

By varying optical devices strain measurements can be performed over a range of length scales. Additionally, this method can be used for both quasi-static as well as high strain rate testing. Since the DIC measurement method is a contact-free technique this method is well suited to examine the complex damage and failure behavior of braided composite structures.

3 X-ray Based Methods for Braided Composites

Computed tomography (CT) is an X-ray based imaging technique that allows for the internal structure of an object to be investigated by non-destructive means [52]. There is a wealth of data and research that exists for the application for this advanced measurement method. The imaging technique has been used extensively by the medical community to investigate physiological structures for diagnostic purposes [53]–[55]. CT scans provide accurate geometric analysis of three dimensional structures. In addition, materials of different density can be identified through their absorption of X-rays.

As conventional CT machines usually have resolutions in the millimeter range, investigation of matrix-fiber bonding as well as void content determination can be challenging in CT machines. Micro-computed tomography (μCT) measurement technique offers an alternative in these scenarios. μCT measurements typically have a resolution below 50 micrometers (μm). A detailed review of the micro-computed tomography (μCT) measurement technique was performed by Stock [56]. The difference in resolutions is due to the fact that conventional CT machines are designed for rapid scanning of patients whereas μCT machines are not limited by scan time allowing for higher resolutions to be achieved. A schematic of the μCT imaging process is shown in Figure 9. The setup for a μCT machine differs from medical CT machines [52] . Medical CT machines the source and detector rotates around a stationary patient. For μCT machines, the test sample is rotated and the X-ray source and detector remains stationary.

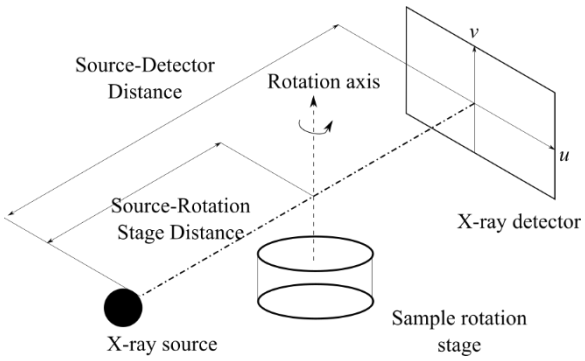

Figure 9: Micro-computed tomography (μCT) schematic

The CT measurement method has also been used for a variety of industrial purposes [57]. Example industrial applications for CT measurements include: additive manufacturing, composite materials, and electrical devices [58]–[60]. CT scanning is considered to be a revolutionary development following coordinate measurement machines (CMMs) [57]. Example applications for the CT measurement for composite material includes reconstruction of curvilinear fiber geometry [61]. New methods and approaches need to be developed to allow for the CT

measurement method to be used for industry specific sample quantification. The CT measurement method has been used for conventional laminated composite and textile composite structures but fewer studies have been performed on 2D and 3D braided composite structures [62]–[65].

3.1 Micro-Computed Tomography

The computed tomography method can provide a wealth of information for braided composite structures. Addition to the interfacial bonding characteristics and void content, this method can also be used to accurately characterize the internal yarn and matrix architectures of both 2D and 3D braided structures. Accurate measurement of braid geometry is necessary for improving current analytical and numerical models. The μCT method has already been used, and gaining increasing popularity, to investigated the yarn architecture of textile composite structures [63]–[65]. The same methodology that has been used for textile composites can be applied to the investigation of yarn architecture for braided composite structures. Additionally, this method can be used to accurately quantify the presence of voids and inclusions in composite structures in 3D [62].

Although no publications are currently available, in the near future this method can be used for damage detection in braided materials. Since the μCT method is a non-destructive measurement this technique is ideally suited to the assessment of damage within braided structures. Samples can be examined before and after damage allowing for failure mode investigation. In-situ deformation and strain can also be obtain by combining μCT measurements with a digital volume correlation analysis technique [66].

3.1.1 Braid Geometry Using μCT method

The geometry of tubular braided composite structures using μCT method were assessed by Melenka *et al.* [67]. The braid preforms used in this study were fabricated using 5680 denier

Kevlar 49 yarns and embedded in an epoxy matrix (Epon825/Ancamine1482). Authors indicated the importance of the selection of X-ray beam energy to allow for identification of the constituent materials within the braided structures.

In the work by Melenka *et al*, the paths of individual yarns within a Diamond (1/1) braided composite were identified which was never shown in the literature before. An image segmentation procedure was used to identify the individual yarns within the braid in order to identify yarn path. To assess each of the braid yarns the cross-sectional area, aspect ratio, braiding angle and fiber undulation period were determined. An example of the idealized braid geometry that is commonly used for modeling the mechanical properties of tubular braided composites is shown in Figure 10. In addition, a cross-sectional image of a braided composite samples is included in Figure 10. Measurement of yarn cross-sectional area, aspect ratio, braiding angle and fiber undulation period are necessary for improving current tubular braided composite analytical and finite element analysis models. The calculations of the theoretical yarn undulation length, p, and yarn aspect ratio, $a_{r,}$ are shown in equations (1) and (2).

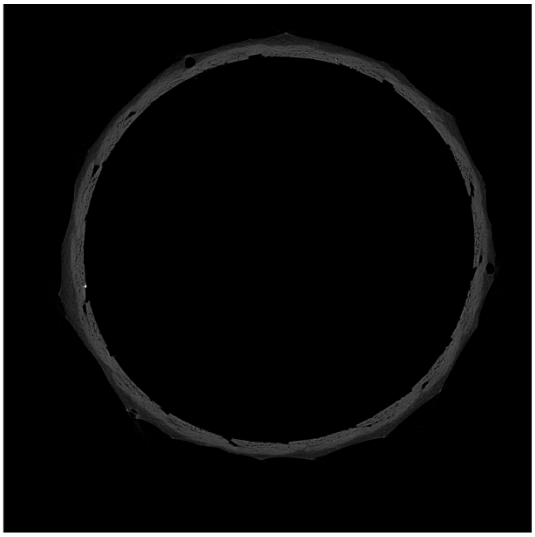

μCT cross section of a braided composite

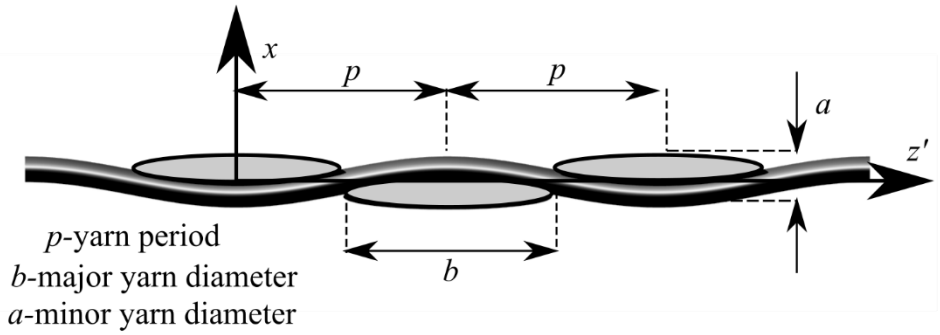

Figure 10: Braided composite μCT cross-section and idealized yarn geometry used for tubular braid modeling

$$a_r = \frac{a}{b} = \frac{\pi ab}{\pi b^2} \quad (1)$$

$$p = \frac{r_0 \beta}{2 sin\alpha} \quad (2)$$

$$\beta = \frac{2\pi}{n}$$

The internal structure and porosity of three dimensional full five-directional (3DF5D) braided composite structures was examined by Ya *et al.* [68]. 3DF5D braided composite are advanced structures which have complex 3D geometry. An example 3D braid is shown in Figure 11 demonstrating the complex yarn architecture. Accurate measurement of the size and orientation of braiding yarns within the 3DF5D structure is crucial for a full understanding, and later modeling,

its properties. Current models that exist for braided composites typically assume elliptical or polygonal cross-sections for braid yarns. Idealized yarn paths are also assumed. Measurement and understanding of braid geometry is important for creating more accurate models for braid geometry. Analysis of complex 3DF5D using the μCT measurement method will allow for yarn size and orientation to be assessed within the braided composite structure. To assess the orientation of yarns within the braided structure glass fiber tracer yarns were introduced. The glass fiber yarns have a lower density than carbon fiber yarns which make up the rest of the braided structure. The glass and carbon fiber yarns have differing X-ray attenuation rates and therefore will have varying grayscale values when examined using the μCT measurement method. Samples were examined using a full rotation of 360° around the sample and the stepping interval is 0.5°. The X-ray source voltage and current were not specified for the 3DF5D composite structures. The size and shape of axial and cross-section of yarns was analyzed from μCT image data. The path of the axial and braiding tracing yarns within the 3DF5D structure were analyzed. In addition, the cross-sectional area of the tracing yarns was also investigated. Axial and braiding yarns ellipticity was calculated to compare the actual yarn cross-sectional geometry with elliptical geometry that is commonly assumed for braid yarns. Ellipticity is measured by determining the ratio of the equatorial and polar radius of an ellipse (3). The average ellipticity of braiding yarns was found to be 2.79.

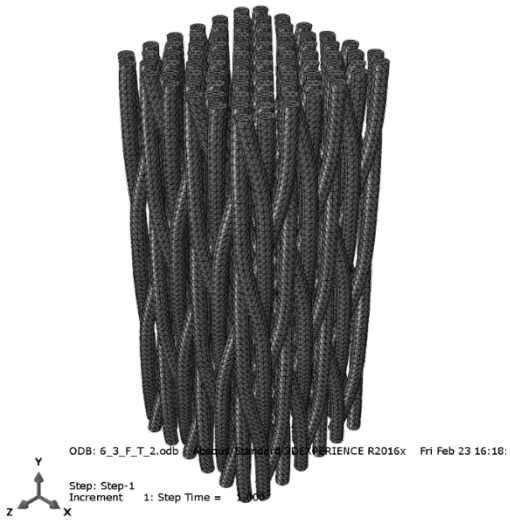

Figure 11: Example 3D braided composite demonstrating the complex yarn geometry.

$$e = \sqrt{\frac{a^2 - c^2}{a^2}} \tag{3}$$

From the μCT measurement yarn geometry was assessed. Internal yarns were found to form a flattened elliptical shape while external yarns have one side that is flattened by the mold used to cure the braided composite.

3.1.2 Braid Damage and Failure

Braided composites possess high damage tolerance and through-thickness strength due to the interwoven nature of the braiding yarns [69], [70]. Braided composites exhibit improved damage tolerance over conventional laminated composites and woven textile composite structures [71]. The complex three dimensional nature of braided composites presents challenges for assessing damage and failure. Braided composites can exhibit a number of failure modes including: matrix failure, delamination, tow splitting, and tow facture. Measurement of damage and failure of braided composites is necessary to improve existing models. Damage and failure must also be assessed for a variety of loading conditions. The X-ray based μCT is well suited for the assessment of damage and failure to braided composite structures.

One of the first studies to examine 2D braids' failure using X-ray based measurements was Ivanov *et al*. [72]. In this work, Triaxial diamond (1/1) braided composites were examined using a Philips HOMX 161 Microfocus X-ray system. Braid samples were loaded in both the longitudinal and transverse direction and then inspected using the X-ray measurement system. The braid samples were immersed in a diiomethane solution to assist in the identification of cracks within the braided composite structures.

From this study it was found that cracks that form do not cross the entire specimen at once, i.e. the cracks are blunted due to the interlocked internal structure of the braided preforms. It was also determined that crack formation exhibits a competitive mechanism between crack length growth and crack density increase. In the study, damage levels were also assessed using acoustic emission. Two damage stages observed: (1) transverse crack initiation registered by acoustic emission; (2) progressive crack density growth and delamination initiation.

Damage to 3D braided structures was examined by Kim *et al.* [73]. Damage was assessed using the X-ray μCT measurement method. The braid samples were scanned using a Skyscan 1172 with an X-ray source of 40kV and 200 μA. The μCT image were used to observe the damage mechanism that occurred within the braided composite sample at five different loading stages. Transverse cracking and micro-delamination were observed.

The effect of impact and damage on hybrid 2D braided composites was examined by Sutcliffee *et al.* [74]. In this work braids were fabricated in a Regular (2/2) configuration. Varying quantities of carbon and glass fibers were introduced to manipulate the impact resistance of the braided structures. An example of a hybrid braided composite structure is shown in Figure 12. Samples were produced with 50, 75 and 100% carbon fiber tows.

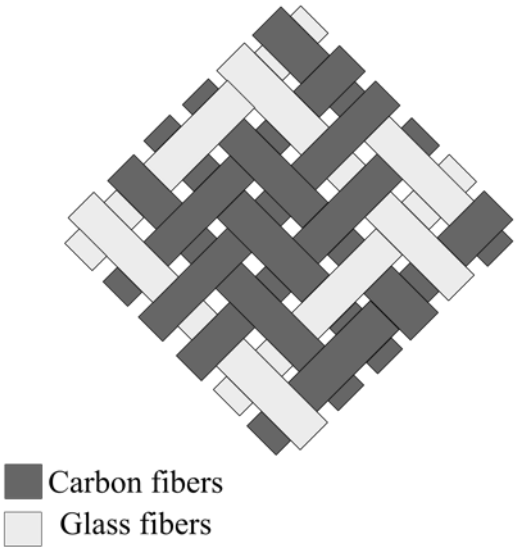

Figure 12: Schematic of hybrid braid with carbon and glass fiber tows. Adapted from *Sutcliffee* et al. [74]

Impact tests were performed on the test samples using impact energies up to 50J. Velocities of the impactors ranged from 46 and 83m/s for the heavy and light impactors respectively. Damage to the braided samples was assessed using the µCT measurement method. The braid samples were scanned using resolutions of 6.2 and 9.9 µm and a beam energy of 70 kV at 90 µA was used with a 2 second exposure. All braid samples were emerged in a zinc iodide solution for 5 minutes before scanning to assist in micro-crack detection. In addition to the µCT measurement method, contact profilometry, ultrasonic C-scanning and vibration measurement methods were also used to assess sample damage.

The results from the µCT measurements indicated that internal damage could be assessed using this measurement method. It was also noted that the zinc iodide solution was an effective approach to enhance crack detection. Matrix cracking leading to delamination and tow splitting was also observed from the µCT measurements.

By varying the quantity of carbon fiber within the braided structures was found to decrease the sample density by 12% for a 50:50 glass-carbon fiber braid compared to a 0:100 glass-carbon

braid. Damage to the 50:50 glass-carbon fiber braid was significantly smaller than the 25:75 and 0:100 glass-carbon fiber braids. These results indicate that the formation of hybrid braids can lead to improved impact resistance by compromising density and axial stiffness.

The study by Zhang *et al.* examined the effect of thermal cycling on triaxially braided composite structures [75]. Samples were fabricated using six layers of Toray T700s yarns with two epoxy resins, 3502 and PR520. The samples in this work were thermally cycled between -55°C and 120°C using a thermal chamber. All samples underwent 160 thermal cycles. X-ray contrast of the braid samples was enhanced by immersing the test samples in a zinc iodide/alcohol/ water solution. To examine the effect of thermal cycling X-ray μCT measurements of the test samples were performed. Micro-cracks were observed in test samples after 50 thermal cycles were applied. Micro-cracks were observed in the direction of fiber orientation for both the longitudinal and biaxial yarns.

The μCT measurements of the braid samples were used to quantify the micro-crack distribution in each sample. The micro-crack density was assessed for each of the six braided composite layers. Higher crack densities were observed in the inner layers compared to the external braid layers.

The work by Zhang *et al.* also demonstrates the use of the μCT measurement method to examine the effect of thermal cycles on triaxially braided composite structures. Braided composites, much like conventional laminated composites, are affected by temperature effects and the μCT analysis technique allows for investigation of the effect of temperature on the micro-structure of braided composite structures.

The effect of impact and damage on 3D braided composites was examined by Li *et al*. [76]. A schematic of the test setup and tubular sample is shown in Figure 13. A Split Hopkinson bar test

was used to perform impact on the braided composite samples. Samples examined in this work were manufactured using a 4-step 3D braiding procedure and curing using vacuum assisted resin transfer molding (VARTM). Carbon fiber T700-12k yarns and JC02A and JC02B resins were used to create the braided structures. 3D braided composites have improved through thickness properties compared to 2D laminates and textile composites. Two braiding angles were used to produce samples in this work: 25 and 35°. Varying strain rates were achieved by manipulation of the gas pressure level used. Gas pressures of 0.3, 0.6 and 1.0 MPa were used to achieve varying strain rates.

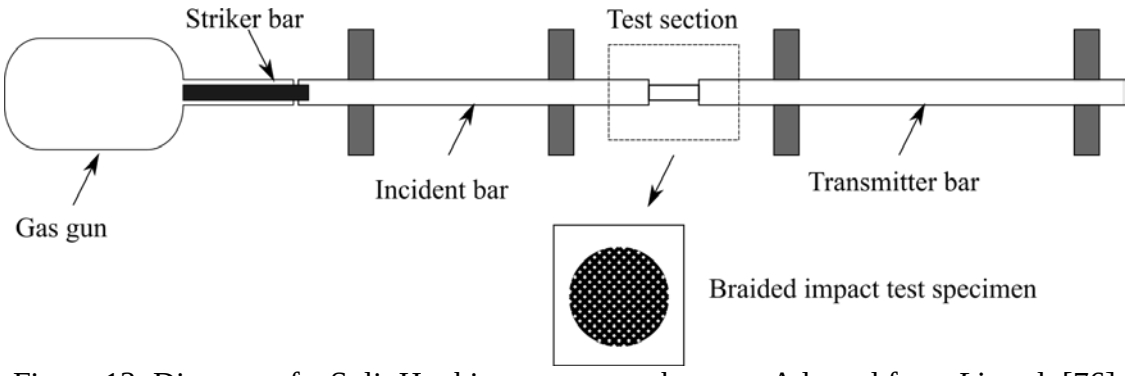

Figure 13: Diagram of a Split Hopkinson pressure bar test. Adapted from *Li* et al. [76]

After impact, samples were inspected using the µCT measurement method. Samples were examined using a Skyscan 1172 µCT. A 0.4°rotation was used step was used and a source voltage of 40 kV at 250µA was utilized. A random movement process was utilized to aide in ring artifact minimization. The collected µCT images of the braid samples were used to inspect the damage and failure modes that occurred due to impact of the 3D braided composite samples. The collected results indicated that damage to braid is influenced by impact velocity and braid geometry. Additionally, braids with a higher braid angle were found to have greater impact resistance due to the packing/ tightness of the braiding yarns.

The effect of impact and damage was also examined by Zhou et al. where 3D tubular braided composite examples loaded under transverse impact [77]. In this work, a split Hopkinson bar was used to create impact loading of the tubular samples. An example of a damaged braid sample impacted by a projectile is shown in Figure 15.

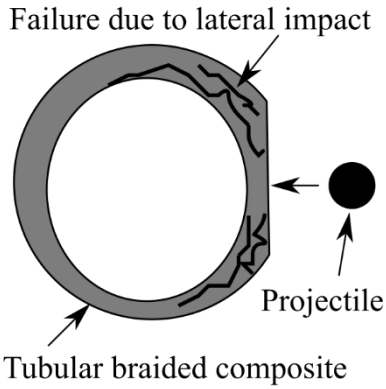

Figure 14: Schematic example of lateral damage to a braided composite structure

Three different numbers of braiding layers (2 layers, 3 layers and 4 layers), as well as three different braiding angles (15, 30 and 45°) were examined in this study. Carbon fiber T700-12K tows were used to form the braided structure. Epoxy resin was employed to consolidate the braided composites with the vacuum-assisted resin transfer molding (VARTM) manufacturing technique. Transverse impacts with 7 m/s, 12 m/s and 17 m/s velocities were used.

A Zeiss MicroXCT-400 µCT was used to examine the tubular braid samples. The X-ray source voltage and current was not specified. As well, the number of projections was also not provided for the tubular braid samples. Using µCT images the effect of braiding angle and number of braid layers was explored. Results showed that increasing braid layers improved impact resistance. Failures that were observed in the braid samples were: resin cracking, tow splitting, de-bonding between yarns and fiber breakage.

The µCT measurement method is an important tool for investigating and evaluating damage to braided composite structures. Since the µCT method is a non-destructive measurement it is well suited for the investigation of damage and failure of braided components. Fracture surfaces and damage severity and be assessed through this measurement technique. In addition, the µCT method can be used to effectively quantify the 3D architecture of both 2D and 3D braided composite structures. Features that can be quantified with the µCT include: yarn width, yarn thickness, yarn undulation period, braid angle, fiber volume fraction, matrix volume fraction, void volume fraction, and void distribution. All aforementioned braid measurements are necessary for accurate model development and quality control of braid manufacturing.

3.1.3 Void detection using µCT

The measurement and identification of voids and inclusions within braided composite structures is important to ensure consistent performance. Some of the earliest work on void measurement of braided composites was performed by Kruesi and Hasko [78]. In this work void volume fractions were found to range from 1.74–3.71% and were measured using conventional void measurement methods. Conventional void measurement techniques like acid digestion and matrix burn off can provide information on the quantity of voids or inclusions within the braid structure however, data on void size and distribution cannot be determined using this method. Microscopy techniques have also been used to assess voids within braided composites but these measurements only allow for the analysis of voids within a 2D cross-section [79]. The 3D size and distribution of voids are necessary for the accurate prediction of mechanical properties using advanced modeling techniques. Void size and distribution data is also required for quality control and manufacturing purposes.

A number of researchers have explored the effect of voids using advanced FEA simulations for braided composites. The effect of voids on the mechanical properties was explored by Xu and Qian [80]. In this work a FEA model was created where random voids were introduced within the braided composite structure and the effect of voids on mechanical properties were explored. Similarly, the study by Dong and Huo examined the effect of voids and internal defects on 3D braided composite structures [81]. The effect of voids as well as braiding angle and fiber volume fractions were explored on the elastic properties of braided structures. It was determined that voids within fiber tows had a more significant effect on mechanical properties than voids within the matrix material. The result of these FEA studies demonstrates the effect of voids on braid mechanical properties and provides motivation for the minimization of defects in the braid manufacturing process.

The μCT measurement method has been utilized to examine voids within braided composite structures. The examination of voids provides necessary data for models to predict the mechanical properties of braided composite structures. Additionally, void measurement provides useful data for the quality control and manufacturing of braided composite structures.

Voids were analyzed by using a threshold-based (thresholding) method by Ya *et al.* for 3DF5D braided composite structures [68]. A sensitivity analysis was performed to examine the effect of thresholding levels on voids identified within the braided structure. Several thresholds used to study effect of thresholding on void identification. Voids were found mostly in the matrix regions of the braided composite structure. Author's did not comment on the reason for increase in void content with threshold value which is an important point; however, both enclosed and elongated voids within the braid structures were included in the study.

Voids in tubular braided composites were examined by Melenka *et al.* [82]. In this work Kevlar49 Epon825/Ancamine1482 epoxy braided composites were examined using the µCT measurement method. Void content of the braided composite sample was examined using an image segmentation method. For the braided composite sample examined in this work a void volume fraction of 2.44% was determined. An example braid cross-section obtained from a µCT measurement is shown in Figure 15. Enclosed voids and open pores were identified as voids within the composite braid. Void and inclusion measurement is vital to reduce failure initiation sites in braided composite structures. Manufactures require the ability to identify voids, pores and holes. Holes represent regions where no fiber or matrix is present while pores indicated that sufficient matrix has not penetrated into the center of the braid.

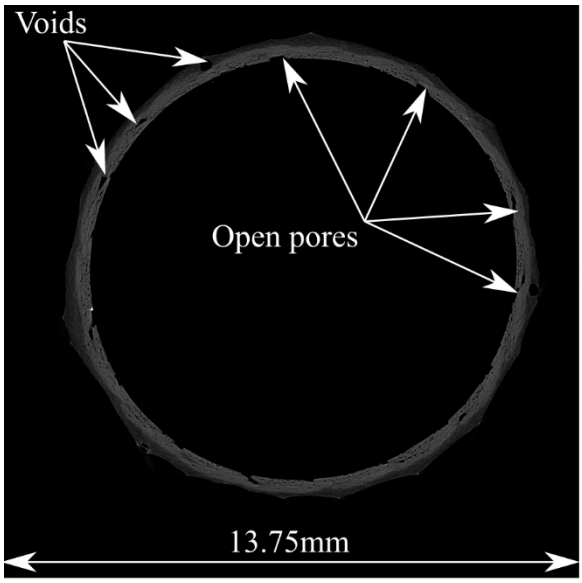

Figure 15: Example braided composite cross-section obtained from a µCT measurement. Open pores observed along the inside diameter of the braid. Enclosed voids are also present within the braid yarns

The effect of voids on cellulose fiber braided composites was also explored by Melenka *et al*. [83]. In this work, Regular (2/2) braids with two braiding angles (35 and 45°) were investigated. A 1.0µm^3 voxel size was used in this work to investigate the microstructure of the two braided samples. The total void volume fraction of the 35 and 45° braids was found to be 1.34 and 1.82%

respectively. In this work the major and minor diameters of individual fiber tows were also examined. This work demonstrates the assessment of braided composite geometry using the μCT measurement technique.

3.1.4 Digital Volume Correlation

In the previous sections, the CT measurement method has been used to examine failure and defects in braided structures as well as to quantify geometric details such as yarn size, yarn orientation and matrix volume. These techniques fall under the umbrella of quantitative x-ray tomography [60]. Advanced techniques are emerging related to computed tomography. Quantitative x-ray tomography methods are concerned with acquiring three dimensional measurements utilizing the CT imaging method.

An example of a quantitative CT method which is an extension of the 3D DIC, discussed in section 2.1.2, measurement technique is known as Digital Volume Correlation (DVC) [84], [85]. DVC allows for the measurement of volumetric strain throughout a sample. The DVC measurement method is commonly used in conjunction with computed tomography (CT) to collect volumetric data for a sample. The DVC measurement method has been used for the measurement of volumetric strain in trabecular bone and conventional composite laminates and to measure three dimensional plant root growth [66], [86]–[89]. Presently, few studies have applied the DVC measurement method specific to composite materials [90], [91]. The internal strain fields of braided composite structures have not been investigated using the DVC measurement method. A schematic of the DVC analysis procedure is shown in Figure 16. The DVC measurement method requires the collection of a reference CT dataset as well as a dataset after load or deformation has been applied to the specimen. A cross-correlation algorithm is used to quantify deformation between the reference and deformed CT datasets [84], [92], [93]. The cross-correlation algorithm is similar to the DIC cross-correlation algorithm described in Section 2.

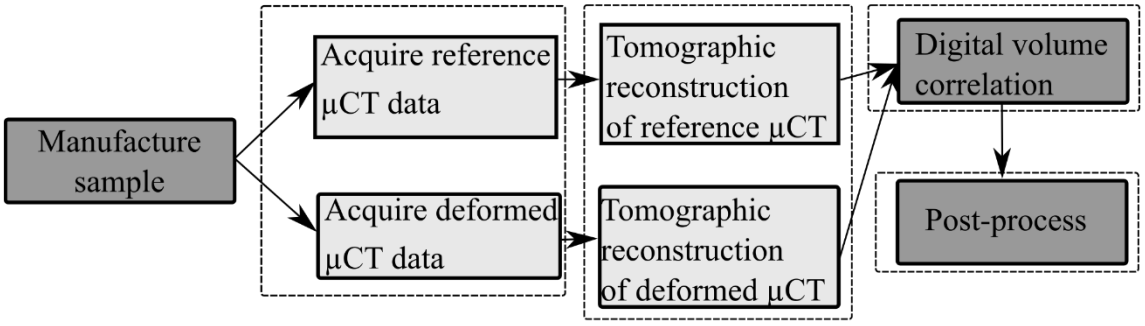

Figure 16: Schematic of the Digital Volume Correlation (DVC) analysis method

One of the first studies attempted to utilize the DVC measurement method was performed by Melenka [94]. In this work a compressive load was applied to a tubular braid sample and the volumetric deformation and strain of the braid sample was observed using the DVC measurement method. This method will be vital for better understanding the in-situ strain that exists within both 2D and 3D braided composite structures.

3.2 Computed Tomography Analysis of Braided Composite Structures

Several studies have examined braided composite structures using the μCT measurement method. Table 3 provides details on the μCT machine, X-Ray voltage, current, voxel size and sample materials examined. Data presented in this table will provide a useful guide for preparing and designing future μCT studies for braided composite structures. Appropriate selection of voxel size enables the resolution of small scale features within braided structures. X-Ray voltage and current settings are selected based on the material density within the braided structure. Table 3 lists common X-ray energy settings to analyze braided structures.

Table 4: Computed tomography scan setting for braided composite structures

Author	µCT Machine	X-Ray Voltage	X-Ray Current	Voxel Size	Sample Materials	Manufacturing Method
Ivanov *et al.* [72]	HOMX 161 Microfocus X-ray	Not Specified	Not Specified	Not Specified	Carbon Fiber Rovings	Triaxial braiding
Kim *et al.* [73]	Bruker Skyscan 1172	40 kV	200 µA	Not Specified	UHMWPE Fibers	4-step circular braiding
Sutcliffee *et al.* [74]	Nikon/ Metris HMX	70 kV	90 µA	6.2 and 9.9 µm	Glass/Carbon Fibers	2D braiding
Zhang *et al.* [75]	Not Specified	Not Specified	Not Specified	Not Specified	T700 Carbon Fiber with 3502 and PR520 epoxy resins	Triaxial +60/0/-60° braiding
Li *et al.* [76]	Bruker Skyscan 1172	40 kV	250 µA	4.9µm	3D carbon/epoxy braided composites	3D braiding
Zhou *et al.* [77]	Zeiss MicroXCT-400	Not Specified	Not Specified	20.11µm	T700-12k tows	4-step circular braiding

Ya *et al.* [68]	XM-Tracer-255	Not Specified	Not Specified	10 µm	3DF5D braids with carbon and glass fibers	4-step braiding
Melenka *et al* [67]	Bruker Skyscan 1076	51kV	110 µA	18.2 µm	Kevlar49/Epoxy	Biaxial braiding
Melenka *et al.* [83]	Bruker Skyscan 1272	40kV	200 µA	1.0 µm	Cellulose Fibers/ Bio-based epoxy	Biaxial braiding
Melenka [94]	Bruker Skyscan 1272	40kV	200 µA	3.0 µm	Cellulose Fibers/ Bio-based epoxy	Biaxial braiding

The µCT measurement method can provide significant data on the internal structure and geometry of both 2D and 3D braided composite structures. Accurate measurement of yarn size and geometry is vital for the accurate analytical and numerical modeling of braided composite structures. Furthermore, accurate segmentation of matrix and fiber within the braid geometry is necessary to for the prediction of matrix and fiber volume fractions. Finally, the µCT measurement process can also be used to accurately quantify the 3D void content of braided structures. The µCT measurement method provides accurate 3D information on braided structures whereas conventional optical microscopy or scanning electron microscopy only allows for the assessment of 2D images of braid cross-sections. Furthermore, the µCT measurement of braided composites

can be coupled with cross-correlation techniques described above in order to measure volumetric deformation and strain.

4 Structural health monitoring and embedded sensors

A variety of structural health monitoring (SHM) techniques have been applied to composite structures. A comprehensive review of these SHM methods has been described by Amafabia *et al.* [95]. Additionally, an overview of fiber optic sensors for composite materials has been presented by Ramakrishhnan *et al.* [96]. Although there are a large number of SHM techniques that can be utilized for composite materials, braided composite structures present unique instrumentation and measurement challenges. Unlike conventional laminated composites, braiding is an automated manufacturing process which prevents rapid integration of sensors during the braid manufacturing process. Additionally, the density, size, orientation and undulations of yarns also must be considered when integrating sensors within braided structures.

SHM of braided composite structures has been examined using three main techniques: optical fibers, conductive fibers and acoustic emission. Each of these methods allow for monitoring of damage and failure for braided composite structures. Due to the woven or textile nature of braided composites “Smart Textile” methodologies can be implemented to achieve sensing within braided structures [97]–[99]. The functionalization of yarns within braided structures can allow for health monitoring and the integration of other electronic devices such as illumination [100]. The incorporation of sensors or additional materials in braided composite structures results in Multifunctional Material Systems which further extends range of applications for braided composites [101]–[103].

4.1 Optical Fibers - *Fiber Bragg Gratings*

Optical fibers have commonly been used to achieve health monitoring in composite structures due to their small diameter and low density [104]. The most common optical fiber sensing methods for discrete measurements are Fiber Bragg Grating (FBG) and extrinsic Fabry-Perot interferometer sensors (EFPI) [105]. Fiber Bragg Gratings (FBG) use the variation of the local refractive index of an optical fiber to achieve strain measurement [96]. A schematic of an optical fiber with a Bragg grating is shown in Figure 17. The Bragg grating alters the refractive index of the optical fiber are inscribed on the optical fiber using an ultraviolet laser. As strain is applied to the optical fiber changes to the period of the Bragg grating that occur. The Bragg-wavelength, λ_B, depends on the effective index of refraction, n_0, and the Bragg period, Λ, as shown in equation (4). The change wavelength due to strain is given by equation (5). In this equation, ΔL represents the change in length of the optical fiber and $\Delta\lambda_\epsilon$ is the change in Bragg wavelength due to an applied load. Similarly, temperature change can be detected using (6). Here, ΔT represents the change due to temperature and $\Delta\lambda_T$ is the Bragg wavelength change that occurs due to changes in temperature. FBG sensors can be used to achieve localized strain measurements. Multiple Bragg gratings can be applied to a single optical fiber allowing for multiplexing so that strains can be measured at numerous locations along the sensor length.

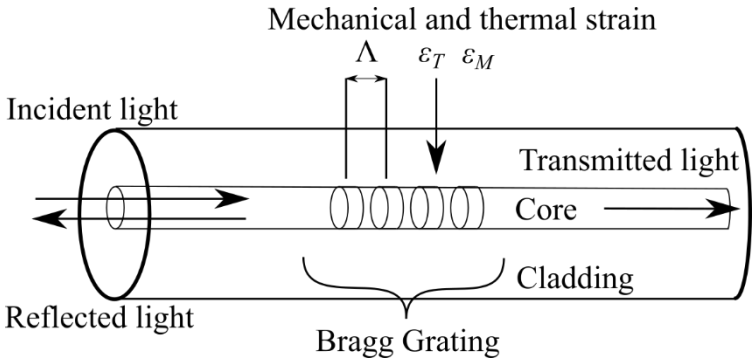

Figure 17: Fiber Bragg grating schematic for mechanical and thermal strain measurement

$$\lambda_B = 2n_0\Lambda \tag{4}$$

$$\Delta\lambda_\epsilon = \lambda_B \cdot \left(\frac{1}{\Lambda}\frac{\delta\Lambda}{\delta L} + \frac{1}{n_0}\frac{\delta n_0}{\delta L}\right) \cdot \Delta L \tag{5}$$

$$\Delta\lambda_T = \lambda_B \cdot \left(\frac{1}{\Lambda}\frac{\delta\Lambda}{\delta T} + \frac{1}{n_0}\frac{\delta n_0}{\delta T}\right) \cdot \Delta T \tag{6}$$

The use of FBG sensors for composite structures was discussed by Luyck *et al.* [106]. In this work the advantages and disadvantages of FBG sensors for composite structures was presented. One major issue with FBG sensors is the entry point into the composite structure which can lead to sensor failure. The size of FBG sensors can also cause geometric distortions within a composite material since the typical diameter of FBG sensors is much greater than common composite fiber diameters. FBG sensors can disturb the strain field within composite materials due to their size. Despite these limitations, FBG and other FOS sensors can be an effective thermal and mechanical strain measurement tool for braided composite structures.

Simultaneous strain and temperature measurement was achieved for 3D braided composites using embedded sensors by Rao *et al.* [107], [108] through the use of extrinsic Fabry-Perot interferometer sensors (EFPI) and Fiber Bragg Grating (FBG) sensors. Both sensors were integrated into a housing with small capillaries and mounted to the braided structure. With the combined sensors a strain accuracy of $\pm 20\mu\epsilon$ and temperature accuracy of $\pm 1°C$ was achieved. The process outlined in this work demonstrates the use of a combined FBG/EFPI sensors for both temperature and strain measurement. The in-situ monitoring can be used to monitor temperature and strain during the curing process as well as for mechanical loading.

A combined EFPI/ FBG sensor was also explored by Kosaka *et al.* [109]. In this work the EFPI/ and FBG sensors were embedded within braided structures. Test samples were evaluated under uniaxial tensile and cyclic loadings. Flat braided composite samples were produced using glass

fibers and a custom mold was manufactured for impregnation of the braid samples with a vinylester resin. The FBG and EFPI sensors were embedded in the braid perform prior to sample curing. A schematic of the braid perform with embedded sensor is shown in Figure 18. The diameter of the optical sensors used in this was 125 μm.

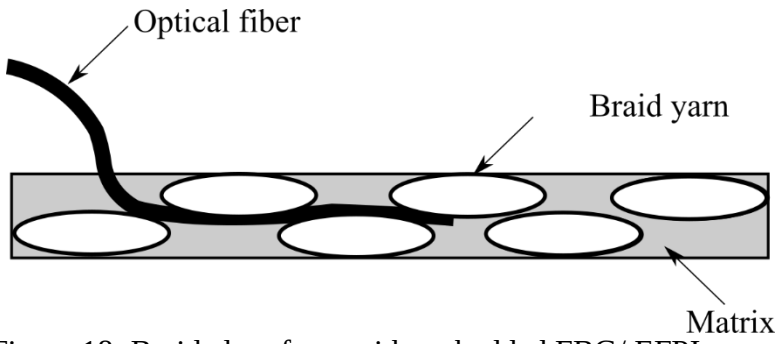

Figure 18: Braided preform with embedded FBG/ EFPI sensor

Sample strain was also monitored during curing by Kosaka *et al.*. This study found that the EFPI/ FBG sensors could only be used effectively for curing monitoring during the cooling process. The EFPI and FBG sensors reported different internal strain results during the heating cycle for the sample. Variations in sensors readings was attributed to the difference in effective stiffness of each of the embedded sensors. Both the EFPI and FGB sensors could be used to accurately measure strain up to 0.8%. After 0.8% strain large errors were observed in the embedded sensor measurement. The FBG and EFPI sensors were also demonstrated to effectively measure strain under a cyclic loading condition.

A co-braiding technique for incorporating optical fibers within braided composite structures was developed by Li *et al*. [110]. In this work, optical FBG sensors were co-braided during the manufacturing process of 3D braids. The FBG sensors were incorporated in the axial direction of the braid and the optical fibers were oriented parallel with the machine braiding direction (Figure 1). The effect of the co-braided optical fibers on the mechanical properties of the 3D braided

structure was explored using a constitutive analytical model. The braids were applied tensile loading, and surface mounted strain gauges were used for comparison with the co-braided optical fiber strain measurements. The tensile test results demonstrated good agreement between the externally mounted strain gauges and internal optical fiber strain measurement. However, an 11% difference between the two strain measurement techniques was reported. The discrepancy between the strain gauges and optical fibers was attributed to the sensor location on the braided structure by the authors as strain gauges were mounted to the external surface of the braid while optical fibers are positioned within the braided structure.

Cure monitoring of 3D hybrid braided composites was examined by Jung and Kang [111]. 3D braided structures were manufactured in both a tubular and flat plate geometry and FBG sensors were embedded by replacing co-braided nylon fibers. The FBG sensors were embedded along both the curved yarns as well as in the machine direction. The FBG sensors used in this study had a diameter of 250 μm. The FBG sensors were embedded after the braid preform was manufactured to avoid damage to the FBG sensor during braiding. Fibers were embedded in the machine direction (longitudinal sample axis) and along the fiber direction. A schematic of the braid samples with fiber embedded in the machine and fiber directions is shown in Figure 19. The placement of FBG sensors shown in Figure 19 demonstrates a major advantage of optical sensors for in-situ strain measurement as fibers can be oriented in either the loading direction or in the braided fiber direction.

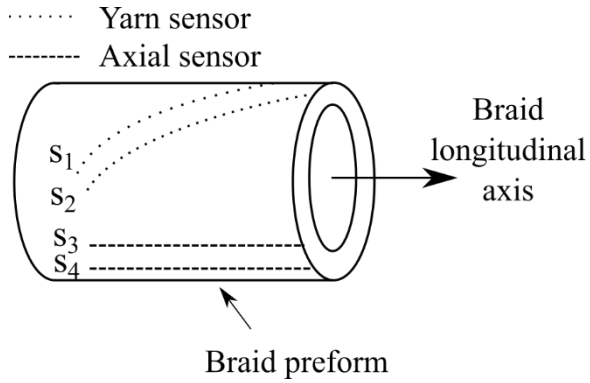

Figure 19: 3D braided composite with embedded FBG sensors. Embedded sensors are oriented in both the axial direction and parallel to the braid yarns.

Compression and three-point bending tests were performed on the 3D hybrid braided samples. The embedded sensors were shown to accurately measure strain under both bending and compressive loading. Dimensional changes to the braided structure was monitored using the curing cycle. The results of the study indicated that FBG sensors can be embedded in 3D braided composites for in-situ strain measurement. The authors noted that there is significant difficulty in embedding the FBG sensors within the 3D braided structure. Dense braided structures or braids which significantly curved yarns may present issues for embedding FBG sensors.

FBG and other FOS sensors are an effective tool for in-situ strain and temperature measurement of braided composites. FBG sensors have been used in braided composite structures for strain measurement and temperature measurement during curing. Challenges associated with FBG sensors and braided composites include: co-braiding optical fibers within a densely packed braided structure [111], [112]. The difference in diameter between the optical fibers and braid fibers can also introduce undesirable strain fields within the braid structure [106]. Optical fibers are also prone to failure while being inserted into braided structures. These technical challenges will need to be overcome to allow for optical fibers to be used as integrated sensors within braided structures.

4.2 Conductive Yarns

Conductive fibers or yarns can also be introduced into braided structures to achieve strain measurement [113]–[115]. The advantage of conductive yarns over optical fibers is that these yarns can easily be introduced in the braiding process. Embedded conductive yarns or fibers utilize the piezoresistive effect to measure strain. Using Ohm's law, the resistance of a yarn can be computed using equation (7). In this equation L represents the static length of the yarn, A is the initial cross-sectional area and ρ is the initial resistivity of the yarn. This allows for the initial resistance, $R_{0,}$ to be computed. The change in resistance of a yarn can be computed using equation (8). In this equation the changes in resistivity, $\Delta\rho$, length, ΔL, and area, ΔA are used to compute the resistance change of the yarn. Using Poisson's ratio, ν_{12}, the area change and change in length can be related to give equation (9). Finally, the gauge factor, G, of the sensor can be determined using (10). The gauge factor can be determined experimentally by applying known strain to the test specimen.

$$R_0 = \frac{\rho L}{A} \tag{7}$$

$$\frac{\Delta R}{R_0} = \frac{\Delta \rho}{\rho} + \frac{\Delta L}{L} - \frac{\Delta A}{A} \tag{8}$$

$$\frac{\Delta R}{R_0} = \frac{\Delta \rho}{\rho} + \epsilon_1(1 + 2\nu_{12}) \tag{9}$$

$$G = \frac{\frac{\Delta R}{R_0}}{\epsilon} \tag{10}$$

The study by Kim *et al.* introduced networks of conductive carbon nanotubes to achieve in-situ strain measurement [73]. Multi-walled carbon nanotubes were distributed within a vinyl ester resin using a three-roll mill calendaring method. Once the customized vinyl ester resin was produced 3D braided composite were fabricated using a vacuum assisted resin transfer molding process. Strain gauges were surface mounted on the braided composite samples for comparison

with the conductive carbon nanotube matrix. Piezoresistive behavior was observed from the embedded carbon nanotube network. As micro-cracks and damage occurred to the braid sample changes reduced electrical resistance was observed. Five characteristic strain stages were observed. The characteristic strains observed were 1) transverse cracks or micro-delamination formation 2) crack growth 4) damage saturation 5) and finally resistance decrease. The five characteristic strain stages were confirmed using X-ray μCT observations. The study by Kim *et al.* demonstrates the methodology to achieve in-situ strain measurement by creating a conductive carbon nanotube network within the braided composite matrix material.

Carbon nanotubes were also introduced as a resistance-based sensing method by Wu *et al.*[116]. 3D braided composite structures were fabricated using E-glass yarns. Carbon nanotubes were dispersed in the epoxy matrix used to form the braided composite. A healant resin was also prepared using a rapid curing resin. Carbon nanotubes within the healant resin were used to sense crack filling. As cracks within the braided structure are filled with the healant resin the electrical resistance changes. The carbon nanotubes introduced in this work were used to both observe damage to the braid samples as well as to measure crack filling using a healant resin.

Structural health monitoring of 3D braided composites was achieved by introducing continuous carbon nanotube threads into 3D braided composite structures by Wan and Guo [117]. Every fourth braid yarn carrier was replaced with carbon nanotube yarns to achieve strain measurement. Strain measurement was achieved by monitoring resistance changes of the carbon nanotube yarns due to an applied mechanical load. Three samples were examined with varying braiding angle, fiber content and density.

A carbon nanotube thread was also embedded in 3D braided composites by Guo *et al.* [118]. 3D braided composite structures were evaluated in response to a three-point bending load. Braids

were manufactured using a 3D braiding process and carbon nanotube yarns were embedded along the longitudinal axis of the braided structure. The embedded carbon nanotube yarns were used to measure longitudinal strain within the 3D braid structure. The sensing carbon nanotube yarns were oriented above and below the neutral axis of the braid sample to measure both tensile and compressive strain when subjected to a three-point bending load. Changes in the resistance of the carbon nanotube sensors were observed for both loading and unloading of the test samples. This work demonstrates the possibility of monitoring damage and failure to 3D braided composite structures under bending loads using embedded carbon nanotube yarns.

Continuous carbon nanotube yarns were introduced into 3D braided composite structures by Ma *et al.* [119]. Four different carbon nanotubes were used with densities that varied from 0.3 g/cm^3 to 1.0 g/cm^3. The carbon nanotubes were introduced in the axial direction of the braided structure. The results from tensile test demonstrated that variations in carbon nanotube density affected the change in resistance measured with the embedded carbon nanotube yarns. The 0.3 g/cm^3 yarns demonstrated the greatest resistance change in response to strain while the 1.0 g/cm^3 yarns. The results of this work demonstrate that the carbon nanotube density can be selected in response to a required strain response.

An integrated sensing method for braided composites was detailed by Legrand *et al* [98]. In this work sensing yarns were prepared by coating glass fibers with a conductive polymer PEDOT:PSS and latex solution at a 7:1 ratio. Terminals were created at the ends of the sensing yarns by coating the yarn with silver paint to allow for an electrical connection. Once the sensing yarns were prepared they were then woven into a braid sample with a 55° braid angle. A tensile test was performed on the braided sample and the change in electrical resistance of the sensing yarn was monitored. The yarn coating methodology presented by Legrand *et al.* demonstrates that

integrated strain measurement can be achieved by functionalizing yarns within the braided structure.

The introduction of continuous conductive yarns has a number of advantages over other health monitoring and sensing approaches. Conductive yarns can be selected to be compatible with the braiding process and therefore will not cause localized distortions which can be caused by sensors such as FBG sensors [106]. Since conductive yarns can be introduced in the braiding process, these yarns can be used to monitor in-situ damage and strain rather than using surface measurements such as strain gauges or extensometers. Additionally, conductive particles can be introduced into braid matrix material to also achieve in-situ strain measurement. Both of these approaches allow for health monitoring of braided composites while using instrumentation approaches that are compatible with the braid manufacturing process.

4.3 Acoustic Emission

Acoustic emission (AE) is a non-destructive sensing technique that is used to monitor the development of defects and cracks in structures [120]. The acoustic emission method monitors stress waves that occur within materials when a load is exerted on a structure. Cracks or fractures will generate stress waves that can then be detected by the AE sensor. A schematic of the AE measurement process for a braided composite structure under a bending load is shown Figure 20.

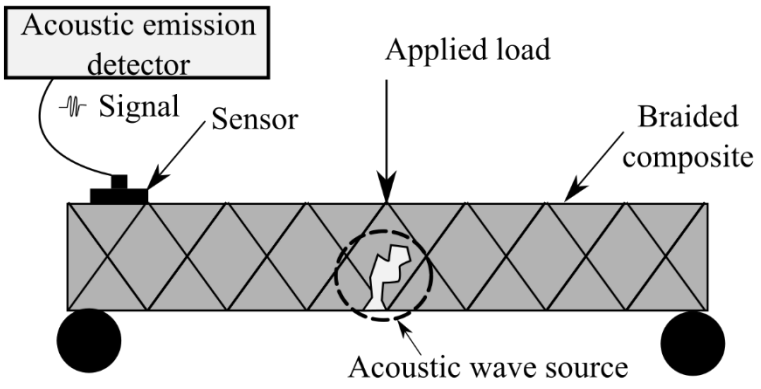

Figure 20: Acoustic emission measurement schematic for a braided composite under three-point bending

The acoustic emission measurement method was utilized with tri-axially braided composite structures by Ivanov *et al.* [72]. The acoustic emission measurements were used to identify the presence of cracks and damage to the tri-axially braided samples.

The AE measurement method was used by Li *et al.* for the monitoring of damage on 3D braided composite structures [121]. The AE waveform was examined in this work for a 3D braid under flexural loading.

Damage to 3D rotary braided composites using AE was performed by Carvelli *et al.* [122]. Abrupt changes to the acoustic emission signal were used to identify damage that occurred to the 3D braided structure. To identify damage, the cumulative energy of the acoustic emission as plotted against stress. These curves can be used to identify a change in the acoustic emission energy as damage. An example AE vs stress plot is shown in Figure 22. The step changes shown in this figure can be used to identify damage events to a braided structure.

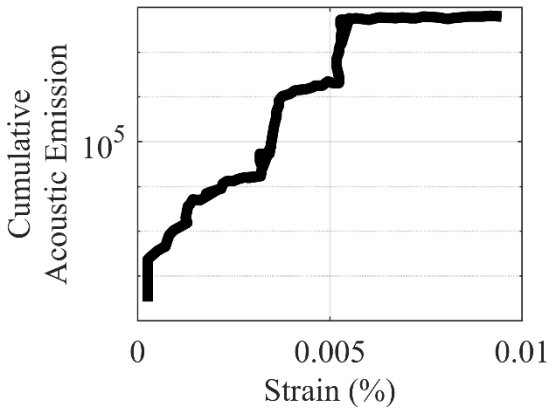

Figure 21: Example Acoustic Emission Cumulative Energy vs Stress Plot

The study by Zhang *et al.* also used the acoustic emission method to examine damage to braided structures [75]. The AE measurement was used to monitor damage to a tri-axially braided structure under thermal cyclic loading. A Weibull distribution was used to fit the experimental normalized cumulative energy and number of cycles. The Weibull distribution equation can then be used to predict the relationship between number of thermal cycles and cumulative acoustic emission. This then allows for damage due to thermal cycling to be predicted.

The AE measurement method was used by Yan *et al.* to examine the post-impact behavior of 3D braided composite structures [123]. Braid samples were first impacted with a 45 J impact and then a compression after impact test was performed. AE signals were used to assess sample damage. The AE method was shown to be an effective tool for examining the failure mechanism of braid samples evaluated using a compression after impact testing approach.

Acoustic emission measurements have commonly been used in conjunction with computed tomography measurements described in Section 3.1 to identify damage and failure that has occurred to test samples.

5 Conclusions

Braiding is a textile based manufacturing process that can be used to create 2D or 3D braided preforms. Braiding is utilized as an advanced and automated composite manufacturing process that can be used to fabricated high performance components highly suitable for critical applications in aerospace, automobile, and biomedical fields. The highly complex interlaced architecture of braided composites requires the use of advanced, accurate, and reliable measurement methods. They include digital image correlation, computed tomography, high speed imaging and structural health monitoring. These methods provide substantial data for measuring and understanding the complex behavior of braided composite structures. Following methods were discussed in detail in this review in an attempt to inform and guide new and existing researchers in the field.

2D and 3D DIC measurement of braided composites is an effective method to examine the complex strain field that occurs due to the interlaced fiber yarns within the braided structures. The DIC measurement method can be utilized for a variety of loading conditions and the measurements can be performed on both the macroscale and microscale of braided structures. DIC measurements can be performed in conjunction with high speed imaging to examine the high strain rate behavior and failure of braided composites structures.

µCT of braided composites provides a wealth of data that cannot be obtained through traditional microstructural analysis methods. Accurate measurement of braid geometry and microstructure, prior and post failure as well as during loading, is necessary to support model development and to examine manufactured braided composite quality – which is made possible with this advanced technique. µCT measurements of biaxial, triaxial and 3D braided composites are necessary to support advanced model development and to improve manufacturing consistence of these complex structures.

SHM of braided composites is required to allow for in-service measurement of braided structures. Damage and failure of composite braids are difficult to predict therefore the inclusion of integrated sensors may improve the utilization of this advanced manufacturing technique. Due to the automated and interlaced nature of braided composites sensors can be readily integrated into braid preforms.

In this manuscript advanced measurement and analysis tools for braided composite structures were discussed. The measurement tools were identified due to their ability to provide extensive data on the behavior and microstructure of advanced braided composite structures. The measurement approaches reviewed in this work are envisioned to become standard analysis approaches for braided composite structures.

6 ACKNOWLEDGEMENTS:

The authors would like to thank the National Sciences and Engineering Research Council (NSERC) for funding support for this work. The authors would also like to thank Mr. Daniel Aldrich for providing the image of a 3D braided composite sample.

7 References

[1] C. Ayranci and J. Carey, "2D braided composites: A review for stiffness critical applications," *Compos. Struct.*, vol. 85, no. 1, pp. 43–58, Sep. 2008.

[2] F. K. Ko, "Braiding," vol. 21, pp. 69–77, 2001.

[3] D. Brunnschweiler, "Braids and Braiding," *J. Text. Inst. Proc.*, vol. 44, no. 9, pp. P666–P686, 1953.

[4] G. W. Melenka *et al.*, "Manufacturing processes for braided composite materials," in *Handbook of Advances in Braided Composite Materials: Theory, Production, Testing and Applications*, 2016, pp. 47–153.

[5] P. Potluri, A. Rawal, M. Rivaldi, and I. Porat, "Geometrical modelling and control of a triaxial braiding machine for producing 3D preforms," *Compos. Part A Appl. Sci. Manuf.*, vol. 34, no. 6 SPEC., pp. 481–492, 2003.

[6] T. D. Kostar and T. W. Chou, "A methodology for Cartesian braiding of three-

dimensional shapes and special structures," *J. Mater. Sci.*, vol. 37, no. 13, pp. 2811–2824, 2002.

[7] Frank K Ko; Christopher M Pastore; Andrew A Head, *Atkins & Pearce Handbook of Industrial Braiding*. Covington, Kentucky, USA: Atkins & Pearce, 1989.

[8] S. C. Quek, A. M. Waas, K. W. Shahwan, and V. Agaram, "Analysis of 2D triaxial flat braided textile composites," *Int. J. Mech. Sci.*, vol. 45, no. 6–7, pp. 1077–1096, 2003.

[9] G. W. Melenka, C. M. Pastore, F. K. Ko, and J. P. Carey, "Advances in 2-D and 3-D braided composite material modeling," in *Handbook of Advances in Braided Composite Materials: Theory, Production, Testing and Applications*, 2016, pp. 321–363.

[10] G. Fang and J. Liang, "A review of numerical modeling of three-dimensional braided textile composites," *J. Compos. Mater.*, vol. 45, no. 23, pp. 2415–2436, Jul. 2011.

[11] A.-M. Harte and N. a. Fleck, "Deformation and failure mechanisms of braided composite tubes in compression and torsion," *Acta Mater.*, vol. 48, no. 6, pp. 1259–1271, Apr. 2000.

[12] A.-M. Harte and N. a. Fleck, "On the mechanics of braided composites in tension," *Eur. J. Mech. - A/Solids*, vol. 19, no. 2, pp. 259–275, Mar. 2000.

[13] L. Xu, S. J. Kim, C. H. Ong, and S. K. Ha, "Prediction of material properties of biaxial and triaxial braided textile composites," *J. Compos. Mater.*, vol. 46, no. 18, pp. 2255–2270, 2012.

[14] X. Ji *et al.*, "Multi-scale simulation and finite-element-assisted computation of elastic properties of braided textile reinforced composites," *J. Compos. Mater.*, vol. 48, no. 8, pp. 931–949, 2014.

[15] D. Goyal, X. Tang, J. D. Whitcomb, and A. D. Kelkar, "Effect of various parameters on effective engineering properties of 2 × 2 braided composites," *Mech. Adv. Mater. Struct.*, vol. 12, no. 2, pp. 113–128, 2005.

[16] J. H. Kim, H. Ryou, M. Lee, K. Chung, J. R. Youn, and T. J. Kang, "Micromechanical Modeling of Fiber Reinforced Composites Based on Elastoplasticity and its Application for 3D Braided Glass / Kevlar Composites," 2007.

[17] C. Ayranci, D. Romanyk, and J. P. Carey, "Elastic Properties of Large-Open-Mesh 2D Braided Composites : Model Predictions and Initial Experimental Findings," *Polym. Compos.*, 2010.

[18] C. McGregor, R. Vaziri, and X. Xiao, "Finite element modelling of the progressive crushing of braided composite tubes under axial impact," *Int. J. Impact Eng.*, vol. 37, no. 6, pp. 662–672, 2010.

[19] C. McGregor, N. Zobeiry, R. Vaziri, A. Poursartip, and X. Xiao, "Calibration and validation of a continuum damage mechanics model in aid of axial crush simulation of braided composite tubes," *Compos. Part A Appl. Sci. Manuf.*, vol. 95, pp. 208–219, 2017.

[20] M. A. Ivey, J. P. Carey, and C. Ayranci, "Manufacturing and characterization of braidtruded fiber reinforced polymer rebar," *Polym. Compos.*, vol. 39, no. 2, pp. 337–350,

2018.

[21] M. A. Ivey, C. Ayranci, and J. P. Carey, “Modeling and Mechanical Characterization of Braidtruded Fiber Reinforced Polymer Rebar,” *Polym. Polym. Compos.*, vol. 16, no. 2, pp. 101–113, 2016.

[22] G. Fang and J. Liang, “A review of numerical modeling of three-dimensional braided textile composites,” *J. Compos. Mater.*, vol. 45, no. 23, pp. 2415–2436, 2011.

[23] J. E. Masters, R. L. Foye, C. M. Pastore, and Y. A. Gowayed, “Mechanical properties of triaxially braided composites: Experimental and analytical results,” *J. Compos. Technol. Res.*, vol. 15, no. 2, pp. 112–122, 1993.

[24] J. E. Masters and P. G. Ifju, “Strain Gage Selection Criteria for Textile Composite Materials,” *J. Compos. Technol. Res.*, vol. 19, no. 3, pp. 152–167, 1997.

[25] B. Pan, K. Qian, H. Xie, and A. Asundi, “Two-dimensional digital image correlation for in-plane displacement and strain measurement: a review,” *Meas. Sci. Technol.*, vol. 20, no. 6, p. 062001, Jun. 2009.

[26] R. A. Naik, P. G. Ifju, and J. E. Masters, “Effect of Fiber Architecture Parameters on Deformation Fields and Elastic Moduli of 2-D Braided Composites,” *J. Compos. Mater.*, vol. 28, no. 7, p. 656, 1994.

[27] R. F. El-Hajjar, S. S. Shams, and D. J. Kehrl, “Closed form solutions for predicting the elastic behavior of quasi-isotropic triaxially braided composites,” *Compos. Struct.*, vol. 101, pp. 1–8, 2013.

[28] I. I. Qamhia, S. S. Shams, and R. F. El-Hajjar, “Quasi-Isotropic Triaxially Braided Cellulose-Reinforced Composites,” *Mech. Adv. Mater. Struct.*, vol. 22, no. 12, pp. 988–995, 2015.

[29] Z. T. Kier, A. Salvi, G. Theis, A. M. Waas, and K. Shahwan, “Estimating mechanical properties of 2D triaxially braided textile composites based on microstructure properties,” *Compos. Part B Eng.*, vol. 68, pp. 288–299, Jan. 2015.

[30] J. P. Johnston, K. C. Liu, M. Yekani Fard, and A. Chattopadhyay, “Mechanical properties and damage characterization of triaxial braided composites in environmental conditions,” *J. Compos. Mater.*, vol. 51, no. 1, pp. 67–80, 2017.

[31] M. a. Sutton, J. H. Yan, V. Tiwari, H. W. Schreier, and J. J. Orteu, “The effect of out-of-plane motion on 2D and 3D digital image correlation measurements,” *Opt. Lasers Eng.*, vol. 46, no. 10, pp. 746–757, Oct. 2008.

[32] N. J. Lawson and J. Wu, “Three-dimensional particle image velocimetry: experimental error analysis of a digital angular stereoscopic system,” *Meas. Sci. Technol.*, vol. 8, no. 12, pp. 1455–1464, 1999.

[33] P. Pollock, L. Yu, M. A. Sutton, S. Guo, P. Majumdar, and M. Gresil, “Full-field measurements for determining orthotropic elastic parameters of woven glass-epoxy composites using off-axis tensile specimens,” *Exp. Tech.*, vol. 38, no. 4, pp. 61–71, 2014.

[34] M. R. C. Fouinneteau and a. K. Pickett, “Shear mechanism modelling of heavy tow braided composites using a meso-mechanical damage model,” *Compos. Part A Appl. Sci. Manuf.*, vol. 38, no. 11, pp. 2294–2306, Nov. 2007.

[35] C. K. Leung, G. W. Melenka, D. S. Nobes, and J. P. Carey, “The effect on elastic modulus of rigid-matrix tubular composite braid radius and braid angle change under tensile loading,” *Compos. Struct.*, vol. 100, pp. 135–143, Jun. 2013.

[36] J. Cichosz, T. Wehrkamp-Richter, H. Koerber, R. Hinterhölzl, and P. P. Camanho, “Failure and damage characterization of (±30°) biaxial braided composites under multiaxial stress states,” *Compos. Part A Appl. Sci. Manuf.*, vol. 90, pp. 748–759, 2016.

[37] T. Wehrkamp-Richter, R. Hinterhölzl, and S. T. Pinho, “Damage and failure of triaxial braided composites under multi-axial stress states,” *Compos. Sci. Technol.*, vol. 150, pp. 32–44, 2017.

[38] D. Zhang, S. Yu, G. Feng, X. Xiao, Q. Ma, and K. Qian, “Numerical Identification of Meso Length-Effect and Full-Field Edge-Effect of 3D Braided Composites,” *Appl. Compos. Mater.*, pp. 1–22, 2017.

[39] G. W. Melenka and J. P. Carey, “Experimental analysis of diamond and regular tubular braided composites using three-dimensional digital image correlation,” *J. Compos. Mater.*, vol. 51, no. 28, pp. 3887–3907, 2017.

[40] C. Wang, A. Roy, Z. Chen, and V. V. Silberschmidt, “Braided textile composites for sports protection: Energy absorption and delamination in impact modelling,” *Mater. Des.*, vol. 136, pp. 258–269, 2017.

[41] R. Böhm *et al.*, “Experimental investigation of the strain rate dependent behaviour of 2D biaxially and triaxially reinforced braided composites,” *Appl. Compos. Mater.*, vol. 21, no. 2, pp. 285–299, 2014.

[42] O. Dorival *et al.*, “Experimental study of impact energy absorption by reinforced braided composite structures: Dynamic crushing tests,” *Compos. Part B Eng.*, vol. 78, pp. 244–255, 2015.

[43] B. Pan, L. Yu, Y. Yang, W. Song, and L. Guo, “Full-field transient 3D deformation measurement of 3D braided composite panels during ballistic impact using single-camera high-speed stereo-digital image correlation,” *Compos. Struct.*, vol. 157, pp. 25–32, 2016.

[44] C. Hampton, F. P., Ko, F. K., Doyle, “Development of ductile-hybrid composites (DHC) by the braidtrusion process,” in *17th International Conference on Composite Materials*, 2009.

[45] F. Hampton, “Cyclic Behavior, Development, and Characteristics of a Ductile Hybrid Fiber Reinforced Polymer (DHFRP) for Reinforced Concrete Members,” Drexel University, USA, 2004.

[46] J. Blaber and A. Antoniou, “Ncorr v1.2,” 2018. [Online]. Available: http://www.ncorr.com/.

[47] D. Z. Turner, “DICe,” *Sandia Report*, 2015. [Online]. Available:

https://github.com/dicengine/dice.

[48] R. Seghir, J.-F. Witz, and S. Coudert, “YADICS (Yet another Digital Image Correlation software),” 2018. [Online]. Available: http://yadics.univ-lille1.fr/wordpress/.

[49] J.-J. Orteu, “3-D computer vision in experimental mechanics,” *Opt. Lasers Eng.*, vol. 47, no. 3–4, pp. 282–291, Mar. 2009.

[50] D. Lecompte *et al.*, “Quality assessment of speckle patterns for digital image correlation,” *Opt. Lasers Eng.*, vol. 44, no. 11, pp. 1132–1145, Nov. 2006.

[51] Y. L. Dong and B. Pan, “A Review of Speckle Pattern Fabrication and Assessment for Digital Image Correlation,” *Exp. Mech.*, vol. 57, no. 8, pp. 1161–1181, 2017.

[52] J. Hsieh, “Introduction,” in *Computed Tomography: Principles, Design, Artifacts, and Recent Advances*, 3rd Editio., vol. 3, Bellingham, Washington: SPIE Press, 2015, pp. 1–23.

[53] M. L. Bouxsein, S. K. Boyd, B. A. Christiansen, R. E. Guldberg, K. J. Jepsen, and R. Müller, “Guidelines for assessment of bone microstructure in rodents using micro-computed tomography,” *J. Bone Miner. Res.*, vol. 25, no. 7, pp. 1468–1486, 2010.

[54] M. Langer and F. Peyrin, “3D X-ray ultra-microscopy of bone tissue,” *Osteoporos. Int.*, vol. 27, no. 2, pp. 441–455, 2016.

[55] M. J. Paulus, S. S. Gleason, S. J. Kennel, P. R. Hunsicker, and D. K. Johnson, “High Resolution X-ray Computed Tomography: An Emerging Tool for Small Animal Cancer Research,” *Neoplasia*, vol. 2, no. 1–2, pp. 62–70, 2000.

[56] S. R. Stock, “X-ray microtomography of materials,” *Int. Mater. Rev.*, vol. 44, no. 4, pp. 141–164, Apr. 1999.

[57] L. De Chiffre, S. Carmignato, J. P. Kruth, R. Schmitt, and A. Weckenmann, “Industrial applications of computed tomography,” *CIRP Ann. - Manuf. Technol.*, vol. 63, no. 2, pp. 655–677, 2014.

[58] A. Thompson, I. Maskery, and R. K. Leach, “X-ray computed tomography for additive manufacturing: A review,” *Meas. Sci. Technol.*, vol. 27, no. 7, 2016.

[59] S. C. Garcea, Y. Wang, and P. J. Withers, “X-ray computed tomography of polymer composites,” *Compos. Sci. Technol.*, vol. 156, pp. 305–319, 2018.

[60] E. Maire and P. J. Withers, “Quantitative X-ray tomography,” *Int. Mater. Rev.*, vol. 59, no. 1, pp. 1–43, 2014.

[61] J. Y. Buffiere, E. Maire, J. Adrien, J. P. Masse, and E. Boller, “In situ experiments with X ray tomography: An attractive tool for experimental mechanics,” *Proc. Soc. Exp. Mech. Inc.*, vol. 67, pp. 289–305, 2010.

[62] J. E. Little, X. Yuan, and M. I. Jones, “Characterisation of voids in fibre reinforced composite materials,” *NDT E Int.*, vol. 46, pp. 122–127, Mar. 2012.

[63] L. P. Djukic, I. Herszberg, W. R. Walsh, G. a. Schoeppner, B. Gangadhara Prusty, and D.

W. Kelly, “Contrast enhancement in visualisation of woven composite tow architecture using a MicroCT Scanner. Part 1: Fabric coating and resin additives,” *Compos. Part A Appl. Sci. Manuf.*, vol. 40, no. 5, pp. 553–565, May 2009.

[64] H. Bale, M. Blacklock, M. R. Begley, D. B. Marshall, B. N. Cox, and R. O. Ritchie, “Characterizing Three-Dimensional Textile Ceramic Composites Using Synchrotron X-Ray Micro-Computed-Tomography,” *J. Am. Ceram. Soc.*, vol. 95, no. 1, pp. 392–402, Jan. 2012.

[65] F. Desplentere, S. V. Lomov, D. L. Woerdeman, I. Verpoest, M. Wevers, and a. Bogdanovich, “Micro-CT characterization of variability in 3D textile architecture,” *Compos. Sci. Technol.*, vol. 65, no. 13, pp. 1920–1930, Oct. 2005.

[66] F. Gillard *et al.*, “The application of digital volume correlation (DVC) to study the microstructural behaviour of trabecular bone during compression,” *J. Mech. Behav. Biomed. Mater.*, vol. 29, pp. 480–499, 2014.

[67] G. W. Melenka, E. Lepp, B. K. O. Cheung, and J. P. Carey, “Micro-computed tomography analysis of tubular braided composites,” *Compos. Struct.*, vol. 131, pp. 384–396, 2015.

[68] J. Ya, Z. Liu, and Y. Wang, “Micro-CT Characterization on the Meso-Structure of Three-Dimensional Full Five-Directional Braided Composite,” *Appl. Compos. Mater.*, pp. 1–18, 2016.

[69] A.-M. Harte and N. a. Fleck, “On the mechanics of braided composites in tension,” *Eur. J. Mech. - A/Solids*, vol. 19, no. 2, pp. 259–275, Mar. 2000.

[70] A.-M. Harte and N. a. Fleck, “Deformation and failure mechanisms of braided composite tubes in compression and torsion,” *Acta Mater.*, vol. 48, no. 6, pp. 1259–1271, Apr. 2000.

[71] J.-H. Byun, “The analytical characterization of 2-D braided textile composites,” *Compos. Sci. Technol.*, vol. 60, no. 5, pp. 705–716, Apr. 2000.

[72] D. S. Ivanov, F. Baudry, B. Van Den Broucke, S. V. Lomov, H. Xie, and I. Verpoest, “Failure analysis of triaxial braided composite,” *Compos. Sci. Technol.*, vol. 69, no. 9, pp. 1372–1380, Jul. 2009.

[73] K. J. Kim *et al.*, “Damage characterization of 3D braided composites using carbon nanotube-based in situ sensing,” *Compos. Part A Appl. Sci. Manuf.*, vol. 41, no. 10, pp. 1531–1537, 2010.

[74] M. P. F. Sutcliffe, C. Monroy Aceves, W. J. Stronge, R. S. Choudhry, and A. E. Scott, “Moderate speed impact damage to 2D-braided glass-carbon composites,” *Compos. Struct.*, vol. 94, no. 5, pp. 1781–1792, 2012.

[75] C. Zhang, W. K. Binienda, G. N. Morscher, R. E. Martin, and L. W. Kohlman, “Experimental and FEM study of thermal cycling induced microcracking in carbon/epoxy triaxial braided composites,” *Compos. Part A Appl. Sci. Manuf.*, vol. 46, no. 1, pp. 34–44, 2013.

[76] Y. Li, B. Sun, and B. Gu, “Impact shear damage characterizations of 3D braided composite with X-ray micro-computed tomography and numerical methodologies,”

Compos. Struct., vol. 176, pp. 43–54, 2017.

[77] H. Zhou, C. Li, L. Zhang, B. Crawford, A. S. Milani, and F. K. Ko, "Micro-XCT analysis of damage mechanisms in 3D circular braided composite tubes under transverse impact," *Compos. Sci. Technol.*, vol. 155, pp. 91–99, 2018.

[78] H. G. H. Kruesi A.H., "Computer Controlled Resin Impregnation for Fiber Composite Braiding," in *Int SAMPE Symp Exhib*, 1987, pp. 309–317.

[79] Y. A. Gowayed, "The Effect of Voids on the Elastic Properties of Textile Reinforced Composites," *J. Compos. Technol. Res.*, vol. 19, no. 3, pp. 168–173, 1997.

[80] K. Xu and X. Qian, "An FEM analysis with consideration of random void defects for predicting the mechanical properties of 3d braided composites," *Adv. Mater. Sci. Eng.*, vol. 2014, 2014.

[81] J. Dong and N. Huo, "A two-scale method for predicting the mechanical properties of 3D braided composites with internal defects," *Compos. Struct.*, vol. 152, pp. 1–10, 2016.

[82] G. W. Melenka, E. Lepp, B. K. Cheung, and J. P. Carey, "Micro-computed tomography analysis of tubular braided composites," *Compos. Struct.*, vol. 131, pp. 384–396, 2015.

[83] G. W. Melenka, B. M. Bruni-Bossio, C. Ayranci, and J. P. Carey, "Examination of voids and geometry of bio-based braided composite structures," *IOP Conf. Ser. Mater. Sci. Eng.*, vol. 406, p. 012012, 2018.

[84] H. Schreier, J. J. Orteu, and M. A. Sutton, "Image correlation for shape, motion and deformation measurements: Basic concepts, theory and applications," *Image Correl. Shape, Motion Deform. Meas. Basic Concepts,Theory Appl.*, no. Vdic, pp. 1–321, 2009.

[85] B. Pan and B. Wang, "A flexible and accurate digital volume correlation method for internal deformation measurement," *Meas. Sci. Technol.*, vol. c, pp. 0–13, 2017.

[86] S. D. Keyes, F. Gillard, N. Soper, M. N. Mavrogordato, I. Sinclair, and T. Roose, "Mapping soil deformation around plant roots using in vivo 4D X-ray Computed Tomography and Digital Volume Correlation," *J. Biomech.*, vol. 49, no. 9, pp. 1802–1811, 2016.

[87] B. K. Bay, T. S. Smith, D. P. Fyhrie, and M. Saad, "Digital volume correlation: Three-dimensional strain mapping using X-ray tomography," *Exp. Mech.*, vol. 39, no. 3, pp. 217–226, 1999.

[88] R. Brault, A. Germaneau, J. C. Dupré, P. Doumalin, S. Mistou, and M. Fazzini, "In-situ Analysis of Laminated Composite Materials by X-ray Micro-Computed Tomography and Digital Volume Correlation," *Exp. Mech.*, vol. 53, no. 7, pp. 1143–1151, 2013.

[89] B. K. Bay, "Methods and applications of digital volume correlation," *J. Strain Anal. Eng. Des.*, vol. 43, no. 8, pp. 745–760, 2008.

[90] F. Mortazavi, E. Ghossein, M. Lévesque, and I. Villemure, "High resolution measurement of internal full-field displacements and strains using global spectral digital volume correlation," *Opt. Lasers Eng.*, vol. 55, pp. 44–52, 2014.

[91] P. Lecomte-Grosbras, J. Rethore, N. Limodin, J. F. Witz, and M. Brieu, “Three-Dimensional Investigation of Free-Edge Effects in Laminate Composites Using X-ray Tomography and Digital Volume Correlation,” *Exp. Mech.*, vol. 55, no. 1, pp. 301–311, 2015.

[92] E. Bar-Kochba, J. Toyjanova, E. Andrews, K. S. Kim, and C. Franck, “A Fast Iterative Digital Volume Correlation Algorithm for Large Deformations,” *Exp. Mech.*, vol. 55, no. 1, pp. 261–274, 2015.

[93] B. Pan and B. Wang, “A flexible and accurate digital volume correlation method for internal deformation measurement,” *Meas. Sci. Technol.*, vol. c, pp. 0–13, 2017.

[94] G. W. Melenka, “Digital Volume Correlation Analysis of Braided Composites,” in *SAMPE 2018*, 2018.

[95] D.-A. M. Amafabia, D. Montalvão, O. David-West, and G. Haritos, “A review of structural health monitoring techniques as applied to composite structures,” *SDHM Struct. Durab. Heal. Monit.*, vol. 11, no. 2, 2017.

[96] M. Ramakrishnan, G. Rajan, Y. Semenova, and G. Farrell, “Overview of Fiber Optic Sensor Technologies for Strain/Temperature Sensing Applications in Composite Materials,” *Sensors*, vol. 16, no. 1, p. 99, 2016.

[97] V. Koncar, *Introduction to smart textiles and their applications*. Elsevier Ltd, 2016.

[98] X. Legrand, C. Cochrane, and V. Koncar, *A complex shaped-reinforced thermoplastic composite part made of commingled yarns with an integrated sensor*. Elsevier Ltd, 2016.

[99] C. Cochrane, C. Hertleer, and A. Schwarz-Pfeiffer, *2 – Smart textiles in health: An overview*. Elsevier Ltd, 2016.

[100] M. Liao *et al.*, “Multicolor, Fluorescent Supercapacitor Fiber,” *Small*, vol. 1702052, p. 1702052, 2017.

[101] A. D. B. L. Ferreira, P. R. O. Nóvoa, and A. T. Marques, “Multifunctional Material Systems: A state-of-the-art review,” *Compos. Struct.*, vol. 151, pp. 3–35, 2016.

[102] C. González, J. J. Vilatela, J. M. Molina-Aldareguía, C. S. Lopes, and J. LLorca, “Structural composites for multifunctional applications: Current challenges and future trends,” *Prog. Mater. Sci.*, vol. 89, pp. 194–251, 2017.

[103] R. F. Gibson, “A review of recent research on mechanics of multifunctional composite materials and structures,” *Compos. Struct.*, vol. 92, no. 12, pp. 2793–2810, 2010.

[104] I. García, J. Zubia, G. Durana, G. Aldabaldetreku, M. Illarramendi, and J. Villatoro, “Optical Fiber Sensors for Aircraft Structural Health Monitoring,” *Sensors*, vol. 15, no. 7, pp. 15494–15519, 2015.

[105] K. T. V Grattan and T. Sun, “Fiber optic sensor technology: An overview,” *Sensors Actuators, A Phys.*, vol. 82, no. 1, pp. 40–61, 2000.

[106] G. Luyckx, E. Voet, N. Lammens, and J. Degrieck, “Strain measurements of composite laminates with embedded fibre bragg gratings: Criticism and opportunities for research,”

Sensors, vol. 11, no. 1, pp. 384–408, 2011.

[107] Y. J. Rao *et al.*, "Application of an improved EFPI/FBG sensor system to simultaneous strain/temperature measurement of advanced 3-D braided composite materials," *Proc. SPIE - Int. Soc. Opt. Eng.*, vol. 4596, no. October 2001, pp. 110–118, 2001.

[108] Y. J. Rao *et al.*, "Simultaneous strain and temperature measurement of advanced 3-D braided composite materials using an improved EFPI / FBG system," *Opt. Laser Eng.*, vol. 38, pp. 557–566, 2002.

[109] T. Kosaka *et al.*, "Strain monitoring of braided composites by using embedded fiber-optic strain sensors," *Adv. Compos. Mater.*, vol. 13, no. 3–4, pp. 157–170, 2004.

[110] X. Li, C. Zhao, J. Lin, and S. Yuan, "The internal strain of three-dimensional braided composites with co-braided FBG sensors," *Opt. Lasers Eng.*, vol. 45, no. 7, pp. 819–826, 2007.

[111] K. Jung and T. Jin Kang, "Cure Monitoring and Internal Strain Measurement of 3-D Hybrid Braided Composites using Fiber Bragg Grating Sensor," *J. Compos. Mater.*, vol. 41, no. 12, pp. 1499–1519, 2007.

[112] M. Selezneva *et al.*, "Manufacturing and Flexural Testing of Composite Braided Hockey Sticks With Embedded Fiber Optic Sensors," in *ICCM International Conferences on Composite Materials*, 2009.

[113] W. Obitayo and T. Liu, "A review: Carbon nanotube-based piezoresistive strain sensors," *J. Sensors*, vol. 2012, 2012.

[114] S. Stassi, V. Cauda, G. Canavese, and C. F. Pirri, "Flexible tactile sensing based on piezoresistive composites: A review," *Sensors (Switzerland)*, vol. 14, no. 3, pp. 5296–5332, 2014.

[115] K. M. Liew, M. F. Kai, and L. W. Zhang, "Carbon nanotube reinforced cementitious composites: An overview," *Compos. Part A Appl. Sci. Manuf.*, vol. 91, pp. 301–323, 2016.

[116] A. S. Wu *et al.*, "Sensing of damage and healing in three-dimensional braided composites with vascular channels," *Compos. Sci. Technol.*, vol. 72, no. 13, pp. 1618–1626, 2012.

[117] L. Wan and J. Guo, "Damage Analysis of Three-Dimensional Braided Composite Material Using Carbon Nanotube Threads," *Exp. Tech.*, no. 2015, pp. 1327–1334, 2015.

[118] J.-M. Guo, L.-Y. Gong, and Y. Liu, "Characteristic analysis of carbon nanotube thread embedded into three-dimensional braided composite under bending load," *Sci. Eng. Compos. Mater.*, vol. 24, no. 5, pp. 791–798, 2017.

[119] X. Ma and X. Cao, "Piezoresistive effect of the carbon nanotube yarn embedded axially into the 3D braided composite," *Results Phys.*, vol. 9, pp. 231–236, 2018.

[120] G. Romhány, T. Czigány, and J. Karger-Kocsis, "Failure Assessment and Evaluation of Damage Development and Crack Growth in Polymer Composites Via Localization of Acoustic Emission Events: A Review," *Polym. Rev.*, vol. 57, no. 3, pp. 397–439, 2017.

[121] L. I. Yi, W. A. N. Zhen-kai, and L. I. Jia-lu, "Research on Acoustic Emission Signal of

Three-dimensional Braided Composite Material,” *2011 Third Int. Conf. Meas. Technol. Mechatronics Autom.*, vol. 3, pp. 1103–1106, Jan. 2011.

[122] V. Carvelli, J. Pazmino, S. V Lomov, A. E. Bogdanovich, D. D. Mungalov, and I. Verpoest, “Quasi-static and fatigue tensile behavior of a 3D rotary braided carbon/epoxy composite.,” *J. Compos. Mater.*, vol. 47, no. 25, pp. 3195–3209, 2013.

[123] S. Yan *et al.*, “Effect of Braiding Angle on the Impact and Post-Impact Behavior of 3D Braided Composites,” *Strength Mater.*, vol. 49, no. 1, pp. 198–205, 2017.